Accepted Manuscript

Hot orogens and supercontinent amalgamation: A Gondwanan example from southern India

Chris Clark, David Healy, Tim Johnson, Alan S. Collins, Richard J. Taylor, M. Santosh, Nicholas E. Timms

PII: S1342-937X(14)00328-1
DOI: doi: 10.1016/j.gr.2014.11.005
Reference: GR 1362

To appear in: *Gondwana Research*

Received date: 1 October 2014
Revised date: 31 October 2014
Accepted date: 2 November 2014

Please cite this article as: Clark, Chris, Healy, David, Johnson, Tim, Collins, Alan S., Taylor, Richard J., Santosh, M., Timms, Nicholas E., Hot orogens and supercontinent amalgamation: A Gondwanan example from southern India, *Gondwana Research* (2014), doi: 10.1016/j.gr.2014.11.005

Hot orogens and supercontinent amalgamation: a Gondwanan example from southern India

Chris Clark[1*], David Healy[2], Tim Johnson[1], Alan S. Collins[3], Richard J. Taylor[1], M. Santosh[4], Nicholas E. Timms[1]

[1]Department of Applied Geology, Curtin University, Perth WA 6845, Australia

[2] School of Geosciences, King's College, University of Aberdeen, AB24 3UE United Kingdom

[3]Department of Earth Sciences, The University of Adelaide SA 5005, Australia

[4]School of Earth Science & Resources, Chinese University of Geosciences, Beijing, China

*Corresponding Author

A/Prof Chris Clark

Department of Applied Geology,

Curtin University,

Perth WA 6845

Australia

Email: c.clark@curtin.edu.au

Phone: +61 (0)8 9266 2446

Fax: +61 (0)8 9266 3153

ABSTRACT

The Southern Granulite Terrane in southern India preserves evidence for regional-scale high to ultrahigh temperature metamorphism related to the amalgamation of the supercontinent Gondwana. Here we present accessory mineral (zircon and monazite) geochronological and geochemical datasets linked to the petrological evolution of the rocks as determined by phase equilibria modelling. The results constrain the duration of high to ultrahigh temperature (>900 °C) metamorphism in the Madurai Block to be c. 40 Ma with peak conditions achieved c. 60 Ma after the formation of an orogenic plateau related to the collision of the microcontinent Azania with East Africa at c. 610 Ma. A 1D numerical model demonstrates that the attainment of temperatures >900 °C requires that the crust be moderately enriched in heat producing elements and that the duration of the orogenic event is sufficiently long to allow conductive heating through radioactive decay. Both of these conditions are met by the available data for the Madurai Block. Our results constrain the length of time it takes for the crust to evolve from collision to peak *P–T* (i.e. the prograde heating phase) then back to the solidus during retrogression. This evolution illustrates that not all metamorphic ages date sutures.

Keywords: Phase equilibria modelling; U–Pb geochronology; High temperature metamorphism; Gondwana supercontinent; southern India.

1. Introduction

The Southern Granulite Terrane (SGT) in peninsular India is characterised by the occurrence of high to ultrahigh temperature (>900 °C) metamorphic assemblages over a length scale of ~500 km, in which elevated temperatures persisted for up to 100 Ma (Cawood and Buchan, 2007; Collins et al., 2014; Collins et al., 2008; Santosh et al., 2006; Santosh et al., 2003). The lack of any geological input of heat from mantle-derived magmas requires an alternative heat source that was long-lived.

There are currently two competing hypotheses to account for the source of heat needed to generate UHT metamorphic conditions on a regional scale. Brown (2007) has suggested that UHT metamorphism may record closure and thickening of continental back arc basins, which are characterised by regions of thinned lithosphere. In this scenario, the extreme metamorphic temperatures are due to high mantle heat flow prior to orogenesis, which are enhanced by thickening of the hot crustal column during orogenesis. The most likely tectonic setting for inversion of a back-arc basin is continental accretion and collision at a magmatic arc, which is consistent with the observation that UHT metamorphism is generated during periods of continental assembly (Brown, 2007; Clark et al., 2014). Another plausible, but less well understood, mechanism suggests that the crust can be heated to UHT conditions by the radioactive decay of heat producing elements (HPE) (Chamberlain and Sonder, 1990; Clark et al., 2011; Goffe et al., 2003; Huerta et al., 1998; McKenzie and Priestley, 2008). In this scenario, high temperatures are the result of heat generated within the thickened crustal column during collisional orogenesis. The numerical models of McKenzie and Priestley (2008) suggest that the attainment of UHT conditions requires crust with higher than average concentrations of HPE(>2 μW^{-3}) (Vila et al., 2010) that is subsequently thickened (a thickening factor of three times in their model) during orogenesis and requires

an incubation time on the order of 60 My (their figure 8). A current natural example of this scenario might be the Himalayan collision system, in which metamorphosed crustal xenoliths sourced from the deep crust of the Tibetan Plateau underwent UHT metamorphism at mid crustal depths (Hacker et al., 2000). The metamorphism associated with large scale collisional systems has previously been investigated through the application of 2D numerical models (Beaumont et al., 2010; Beaumont et al., 2001; Beaumont et al., 2004; Faccenda et al., 2008b; Gerya and Meilick, 2011; Jamieson and Beaumont, 2011; Jamieson et al., 2010; Lexa et al., 2011). The results of these studies suggest that elevated temperatures can be achieved in the orogenic core, where crustal material remains buried for extended periods of time.

The aim of this paper is to investigate the heat source required by the occurrence of regional-scale high temperature metamorphism in the Southern Granulite Terrane through the application of *in situ* microprobe dating techniques and a better understanding of the links between accessory mineral growth and the evolution of the major silicate mineral assemblages (Buick et al., 2010; Clark et al., 2009a; Degeling et al., 2001; Fraser et al., 1997; Kelly and Harley, 2005; Kelsey et al., 2008; Kelsey et al., 2007; Korhonen et al., 2013; Korhonen et al., 2011; Yakymchuk and Brown, 2014). We constrain the duration of UHT metamorphism in the Southern Granulite Terrane through the application of U-Pb geochronometers (monazite and zircon) coupled with the pressure-temperature evolution as constrained using phase equilibria modelling, and propose a viable scenario for heating crust to high or ultra-high temperatures on an orogenic scale.

2. Geological setting

The Southern Granulite Terrane, together with central and eastern Madagascar and Sri Lanka, is considered to form part of the microcontinent of Azania, a terrane that was located between

East Africa (the Congo Craton) and Greater India (the Dharwar Craton) during the amalgamation of Gondwana (Fig 1a-d; Collins and Pisarevsky, 2005). The collision of Azania with East Africa was preceded by the docking of a juvenile intra-oceanic arc, comprised of the Vohibory succession (Collins et al., 2012; Emmel et al., 2008; Jöns and Schenk, 2008) in Madagascar and the Eastern Granulites in Tanzania (Möller et al., 1998), with the Tanzania Craton (part of the Congo Craton). Although it is difficult to constrain precisely the timing of this collision, the rocks of the Eastern Granulites and western Madagascar contain 9-12 kbar metamorphic rocks that have ages that range from 655 – 610 Ma (Jöns and Schenk, 2008; Möller et al., 2000) (Fig. 2a, b). The collision, recording the closure of the backarc basin that separates the juvenile rocks of the Vohibory succession (Collins et al., 2012; Emmel et al., 2008) from Azania, followed shortly afterwards at *c.* 620 Ma, and was accompanied by the intrusion of syn-tectonic stratiform granitoids (de Wit et al., 2001; Meert et al., 2003; Nedelec et al., 1995). Collision of Azania with East Africa resulted in the development of a large orogenic plateau composed of thickened Proterozoic crust (Fig. 2c; Collins et al., 2014; Santosh et al., 2009), within which the rocks of central and eastern Madagascar and the Trivandrum and Madurai Blocks in India underwent a protracted history of high to ultrahigh temperature metamorphism (Fig. 3) with ages of metamorphism ranging between 580 and 510 Ma (Cawood and Buchan, 2007; Collins et al., 2008; Collins et al., 2007b).

The final collision in this part of Gondwana is thought, by some, to record the amalgamation of Greater India with East Africa at 530 Ma along what is now called the Palghat Cauvery Shear System (PCSS; Fig. 2d; Clark et al., 2009b; Collins et al., 2007a; Santosh et al., 2009). This suture zone has been traced into Madagascar along the Betsimsaraka Suture zone (Collins, 2006; Collins et al., 2007a; Collins et al., 2003). In the PCSS this area is comprised of reworked Proterozoic crust (Clark et al., 2009a; Collins et al., 2007b), Neoproterozoic oceanic crust (Santosh et al., 2010; Santosh et al., 2012; Yellappa et al., 2010)

and high-pressure and ultrahigh temperature metamorphic rocks (Clark et al., 2009a; Collins et al., 2007a; Kelsey et al., 2006; Nishimiya et al., 2010; Sajeev et al., 2009; Shimpo et al., 2006). Metamorphism and deformation in the PCSS post-date the metamorphic peak experienced by the rocks further to the south that formed part of the Azania microcontinent. However, the nature of this suture zone is debated, and recent papers by Tucker et al (2011a; 2011b; 2014) and Boger et al. (2014), focusing mainly on the Madagascan extension of the suture, consider it to be a zone of intracontinental reworking of Palaeoproterozoic rocks that make up the southern margin of Greater India.

2.1 Madurai Block

The central and southern Madurai Block, lying to the south of the PCSS (Fig. 1c, d), is dominated by charnockite massifs with Sm-Nd and Rb-Sr whole rock model ages in the range 1340-3170 Ma(Bartlett et al., 1998; Bhaskar Rao et al., 2003; Brandt et al., 2014; Plavsa et al., 2012; Plavsa et al., 2014). The charnockites are well exposed in the Kodiakanal massif where they structurally underlie metasedimentary gneisses that dominate exposed rocks to the south and east. The metasedimentary units, which are the focus of this study, contain detrital zircons with U-Pb age spectra that constrain the deposition of their protoliths to after ~1700 Ma (Collins et al., 2007b) and, for some rocks, possibly as late as the mid-Neoproterozoic (Collins et al., 2007b). Ray et al. (2003; 2008) have documented the volumetric heat production from a range of lithologies within the SGT, obtaining values that range from 1.8-5.5 μWm^{-3} for the igneous and metasedimentary lithologies that comprise the bulk of the currently exposed SGT. The dominant lithologies in the southern part of the SGT are migmatitic metapelitic gneisses (khondalites and leptynites), which have average heat

production values > 3 μWm^{-3}; the igneous rocks (charnockites and granites) have lower heat production values typically between 1.5 and 2.5 μWm^{-3}.

The metamorphic evolution of metasedimentary lithologies from the Madurai Block have been the focus of a number of studies, due largely to the reported occurrence of diagnostic ultrahigh temperature metamorphic assemblages from a number of localities (Braun et al., 2007; Brown and Raith, 1996; Mohan and Windley, 1993; Raith et al., 1997; Sajeev et al., 2001, 2004; Sajeev et al., 2006; Tateishi et al., 2004). The peak metamorphic conditions inferred for the UHT rocks in the SGT are in the range 7-13 kbar and 900-1150 °C, and the rocks are considered to have followed a clockwise *P–T* evolution typical of collisional orogenesis (Fig. 3; Brandt et al., 2011; Braun et al., 2007; Brown and Raith, 1996; Mohan and Windley, 1993; Raith et al., 1997; Sajeev et al., 2001, 2004; Sajeev et al., 2006; Santosh and Kusky, 2010; Tateishi et al., 2004; Tsunogae and Santosh, 2010a, b). The age of metamorphism has been constrained using a number of techniques, with electron microprobe (EPMA) monazite, SIMS U-Pb monazite, U-Pb zircon and Sm-Nd garnet-whole rock analyses yielding ages between 600-480 Ma (Bartlett et al., 1998; Braun et al., 2007; Jayananda et al., 1995; Santosh et al., 2006).

3. Sample description and petrology

In order to constrain the conditions and duration of metamorphism in the Madurai Block two metasedimentary gneisses from different locations (Fig 1d) were collected for detailed analysis. Both samples are diatexitic migmatites in which the proportion of leucosome to melanosome varies widely.

Sample I06-62 – Usilampatti (77˚ 49' 34" E 9˚ 56' 25" N)

Rock exposures near the village of Usilampatti are garnet-bearing migmatites containing discontinuous foliation-parallel leucosomes (Fig. 4a, b). Residual portions (melanosome), which may occur as discrete discontinuous layers, contain conspicuous garnet, sillimanite, cordierite, biotite, spinel and opaque minerals (Fig. 4a). Leucosomes are dominated by quartz, plagioclase and K-feldspar and may contain coarse-grained garnet (Fig 4b). The leucosomes are folded and a strong foliation is present within both the leucosome and melanosome that wraps garnet porphyroblasts (Fig 4a, b). A strongly residual sample of aluminous metapelite (I06-62) was selected for detailed study.

In thin section, sample I06-62 is compositionally and texturally heterogeneous, comprising irregular patches and veins of coarse-grained quartzofeldpathic leucosome (individual grains up to 10 mm across) and (generally) finer-grained melanosome rich in ferromagnesian minerals and sillimanite. Garnet forms highly resorbed anhedral porphyroblasts up to 20 mm across (Fig. 4d). Inclusions of quartz, biotite and sillimanite are generally concentrated in the cores of porphyroblasts and, in the case of biotite and sillimanite, commonly show a strong preferred orientation (Fig. 4f). Matrix sillimanite occurs as prismatic grains up to 2 mm in length that generally occur in clusters. Dark green spinel and magnetite occur together as widely distributed, irregular cuspate grains up to a few millimetres across. Within these composite grains magnetite is volumetrically more abundant than spinel.

Cordierite, which may be intergrown with finer-grained magnetite–spinel, surrounds and separates garnet and sillimanite, which are rarely found in contact (Fig. 4e), and isolates these phases from large grains of spinel/magnetite. In many cases patches rich in cordierite that are several millimetres across contain only small fragments of relict garnet in their cores

(Fig. 4e). In addition to its occurrence as inclusions (Fig. 4f), biotite also occurs as randomly oriented larger grains (up to 2 mm across) and grain aggregates replacing garnet and ilmenite, and rarely at the margins of quartz-rich leucosomes where they are in contact with residual portions of the rock.

These petrographic observations are interpreted to record growth of garnet with biotite and sillimanite along the prograde path, with complete consumption of biotite prior to attainment of peak conditions. Cordierite with or without magnetite/spinel, which replace garnet, are interpreted as having grown during the high *T* retrograde segment of the *P*–*T* path, with late biotite probably recording reaction with small quantities of trapped melt as the rocks cooled to an elevated solidus. Microstructural relationships similar to those described above have previously been described from the Madurai Block by a number of workers, who estimate peak metamorphic temperatures of >950°C at pressures greater than 0.6 GPa temperatures (Fig. 3; Braun et al., 2007; Brown and Raith, 1996; Mohan and Windley, 1993; Raith et al., 1997; Sajeev et al., 2001, 2004; Sajeev et al., 2006; Santosh and Kusky, 2010; Tateishi et al., 2004; Tsunogae and Santosh, 2010a, b).

Zircon and monazite are abundant in sample I06-62. Zircon grains are up to 150 μm in length and occur in a number of textural positions including: (1) within the cordierite corona that surrounds the garnet (Fig. 5a); (2) within late biotite (Fig. 5b); and, (3) growing on the edge of ilmenite grains (Fig. 5b). All these positions are suggestive of zircon growth during the high-temperature retrograde evolution of the rock. Cathodoluminesence (CL) images of zircons from this sample (Fig. 5a) display a variety of textures with the cores having a low CL response and typically elongate morphologies. In most cases the cores display oscillatory zoning or simple, broad zonation (Fig. 5c, d, k). Moderate CL response material forms rims on the oscillatory zone cores (Fig. 5c, d, e, k) or whole grains (Fig. 5f, g, i).

Monazite in sample I06-62 occurs as inclusions within garnet or growing in apparent textural equilibrium with ilmenite and is inferred to have grown on the prograde to peak portion of the *P–T* path (Fig. 6a). Yttrium electron probe maps of monazite from this sample (Fig. 6b-g) show very complicated internal zonation patterns. A generation of high Y monazite is observed within a number of grains and appears texturally early. These are referred to as the cores, but are not always in the central portion of the grains (Fig. 6b, e). A variety of lobate/embayment textures, hereby referred to as rims, with a lower Y response are present throughout all grains with low-Y material also forming complete grains. A single monazite grain with a very high Y response that truncates the lower Y monazite was also observed (Fig. 6g).

I06-79 - Kodaikanal (77° 38' 03" E 10° 13' 30" N)

Exposures alongside the Ganguvarpatti to Kodaikanal road consist of interlayered porphyroblastic garnet-biotite gneisses and garnet-cordierite-sillimanite gneisses containing irregular patches and veins of leucosome (Fig. 7a, b). A sample (I06-79) of residual garnet-biotite gneiss was selected for detailed study.

Garnet porphyroblasts are up to 10 mm across and have irregular corroded margins around which garnet is variably replaced by granular aggregates of cordierite (Fig 7c, d). Garnet contains inclusions of quartz, biotite, prismatic sillimanite and rare grains of opaque minerals, inherited/detrital zircon and monazite. Sillimanite and biotite inclusions may show a preferred orientation (Fig. 7d). Biotite occurs as ragged grains up to 5 mm in length that are distributed more or less evenly throughout the sample and show a weak preferred orientation. Ilmenite and magnetite occur as skeletal grains up to 4 mm across that are commonly associated with biotite. Rare composite grains comprise magnetite with

subordinate green spinel. The matrix comprises plagioclase and K-feldspar that form grains 1–4 mm in diameter with lobate-cuspate grain boundaries, along with rare smaller rounded grains of quartz.

Inclusions in garnet show that the high *T* segment of the prograde path was within the stability field of sillimanite, but the absence of matrix sillimanite suggests this phase was consumed at the metamorphic peak. The peak assemblage in this sample is interpreted to be garnet, biotite, plagioclase, K-feldspar, quartz and ilmenite/magnetite, although some or much of the biotite may be of retrograde origin. Cordierite replacing garnet is interpreted to have grown during high temperature retrogression. Biotite is also observed to be partial replacing cordierite in places (Fig. 7c, d).

Zircon in this sample has a variety of morphologies and sizes up to 200 μm in the longest dimension. The majority of grains have a low CL core that displays oscillatory zoning (Fig. 8a, b). In most cases the core material has high CL response rims that slightly truncate the original zoning (Fig. 8b). A number of equant grains are composed entirely of high CL response material (Fig. 8 c, d)

Monazite is intergrown with ilmenite (Fig. 9a) or as inclusions in garnet (Fig. 9b), suggestive of growth during the prograde–peak segment of the *P*–*T* evolution of the rock. The Y element maps of monazite show a very patchy and convoluted zoning pattern that does not seem to correlate in any obvious way with core–rim structure (Fig 9c, d).

4. Metamorphic evolution

Quantitative constraints on peak pressure-temperature conditions and on the near-peak metamorphic evolution use phase equilibria calculations based on the compositions of samples I06-62 (Usilampatti) and I06-79 (Kodaikanal) as determined by XRF analysis. The

former is a residual aluminous metapelite that lacks extensive hydrous retrograde reaction; the latter contains abundant retrograde biotite, suggesting either subsolidus fluid infiltration or retention of a high proportion of the produced melt. Calculations are in the Na_2O–CaO–K_2O–FeO–MgO–Al_2O_3–SiO_2–H_2O–TiO_2–O (NCKFMASHTO) model system and use the end-member thermodynamic data of Holland & Powell (2011; specifically the updated ds62 dataset generated on 06/02/14) and *a*–*X* models detailed in White et al. (2014).

The pseudosection for sample I06-62 has an elevated solidus (>800 °C), reflecting the residual (melt-depleted) nature of the rock, which shows a step to higher *T* (>900 °C) at around 0.55–0.6 GPa (Fig. 10). Within this sample, the abundance of sillimanite inclusions in the cores of garnet and the absence of any evidence for the former presence of kyanite suggest the prograde field passed through the sillimanite stability field. As the composition used to construct the pseudosection is residual, the diagram cannot be used with confidence to place further quantitative constraints on the prograde evolution. Sample I06-62 contains the inferred peak metamorphic assemblage garnet, sillimanite, ilmenite, spinel/magnetite, K-feldspar, quartz and melt. The appropriate fields for this assemblage in the model system are shown (cross ornament) on Fig. 10, and contain the spinel–magnetite solvus. At temperatures below 1000 °C, this constrains peak conditions to pressures of around 0.6–0.8 GPa and temperatures >850 °C, and predicts retained melt fractions of 3–10 mol.% (≈ vol.%), depending on temperature. Cordierite and most of the finer-grained spinel–magnetite in sample I06-62 are interpreted to record partial retrograde replacement of garnet and sillimanite at high temperatures while the rocks were still melt bearing. These observations and interpretations suggest the high temperature retrograde segment of the *P*–*T* path passed into the lower variance cordierite-bearing fields (dotted ornament on Fig. 10), thereafter

crossing the solidus, consistent with decompression of around 0.2 GPa from the metamorphic peak. A high *T* segment of a *P*–*T* path consistent with the observations is shown on Fig. 10.

The pseudosection for sample I06-79 (Fig. 11a) contains a narrow field for coexisting melt and volatile H_2O ('wet' solidus), suggesting that the LOI-based H_2O content used in this bulk composition is too high. To assess the impact of the water content of the peak field we have constructed a *T*–MH_2O diagram at 0.8 GPa. This diagram demonstrates that there is a negligible effect (<5 °C) on the stability of the lower and upper boundaries of the field as H2O content is reduced. The interpreted peak assemblage of garnet, biotite, K-feldspar, plagioclase, quartz, ilmenite and melt with or without magnetite occupies a field in *P*–*T* space consistent with peak temperatures of 820–860 °C and pressures of 0.6–1.0 GPa (Fig. 11). For the modelled bulk composition, orthopyroxene is predicted to be stable at pressures below 0.7 GPa and at higher *T*. Retrograde cordierite is predicted to grow with a small amount of cooling and decompression from the inferred peak (Fig. 11). A high *T* segment of a *P*–*T* path, consistent with the observations is shown on Fig. 11, which is similar to that inferred for sample I06–62, albeit at slightly lower temperatures.

5. SHRIMP monazite and zircon geochronology

In order to link the evolution of the silicate mineral assemblage with growth of both monazite and zircon, the geochronological analyses were undertaken *in situ* within thin section and grain separates mounted in epoxy using the Sensitive High Resolution Ion Microprobe (SHRIMP) at Curtin University (see Supplementary details for the analytical methods). Complete data tables for zircon and monazite U-Pb analyses can be found in Supplementary Data Tables S.1 and S.2.

5.1 Sample I06-62

A total of 15 zircon U-Pb analyses were performed on sample I06-62, including both cores and rims as identified by CL imaging (Fig. 5). Bright CL cores gave predominantly discordant results (only 1 point shows <10% discordance), with the oldest concordant $^{206}Pb/^{238}U$ spot age being 701 ± 11 Ma (Fig. 12a). Analysis of the 12 zircon rims from this sample define a distinct group with a weighted mean $^{206}Pb/^{238}U$ age of 518± 4 Ma (Fig. 13b) and an MSWD of 0.95. A single analysis of one zircon rim (Fig 5h, z7.1) returned a $^{206}Pb/^{238}U$ age of 585 ± 8 Ma, well outside the analytical uncertainty of the other rim analyses.

Twenty-six U-Pb analyses of monazite from this sample covered a large variety of the textures revealed by Y-element mapping (Fig. 6b-g). In general, the high-Y cores gave the oldest $^{206}Pb/^{238}U$ spot ages that range from 767 ± 12 Ma to 654 ± 10 Ma and do not form a single coherent population. The low-Y monazite shows a younger range with $^{206}Pb/^{238}U$ spot ages from 568 ± 11 Ma to 538 ± 9 Ma with a weighted mean $^{206}Pb/^{238}U$ age of 559 ± 4 Ma (Fig 13a; n=20, MSWD 0.90). A single analysis from the highest Y monazite (spot m16.1) returned the youngest $^{206}Pb/^{238}U$ spot age of 508 ± 8 Ma.

5.2 Sample I06-79

A total of 44 zircon U-Pb analyses were performed on sample I06-79, including both cores and rims as identified by CL (Fig. 8a-d). Low response CL cores gave predominantly discordant results but did yield a number of concordant $^{207}Pb/^{206}Pb$ spot ages of 2640 ± 19 Ma, 2495 ± 6 Ma, 2388 ± 7 Ma, 2343 ± 6 Ma, 2249 ± 7 Ma, 2096 ± 10 Ma, 1946 ± 12 Ma, 1784 ± 6 Ma with five $^{206}Pb/^{238}U$ spot ages between 796 and 686 Ma (Fig. 12b). The remaining fifteen high-CL

response zircon rims and whole grains give a $^{206}Pb/^{238}U$ weighted mean age of 512 ± 4 Ma (Fig. 13d) with an MSWD of 2.2.

Twenty-two U-Pb analyses from two monazite grains in this sample were undertaken (Fig. 9b). The convoluted nature of the zoning patterns means that there has been no attempt to relate individual chemical zones to specific ages. Spot ages range from 596 ± 18 Ma to 516 ± 15 Ma with a weighted mean age of 550 ± 7 Ma (Fig. 13c; n=22, MSWD 2.2).

6. LA-ICPMS geochemistry

Complete data tables for zircon, monazite and garnet trace element analyses can be found in Supplementary Data Tables S.3-S.5.

6.1 Sample I06-62

Zircon

REE analyses of zircon from sample I06-62 show three distinct patterns that can be related to textural setting (Fig. 14a). Zircon rims in the cordierite corona show flat REE trends on a chondrite-normalised plot. Yb_N/Gd_N values are 0.6-0.8, corresponding with Y values of around 84–110 ppm and Eu/Eu* of 0.18-0.35. REE patterns for zircon within retrograde biotite show steeper patterns on a chondrite-normalised plot. Yb_N/Gd_N values are 41-67, corresponding with higher Y values of 663-1113 ppm and Eu/Eu* of 0.29-0.36 (Fig. 14a). Zircon growing on ilmenite has a slope that is intermediate between the biotite- and cordierite-hosted zircon chondrite-normalised Yb_N/Gd_N values are 1.9-4.3, corresponding with Y values of 320-1166 ppm and Eu/Eu* of 0.07-0.28.

Garnet

REE analyses for garnet from this sample were very consistent, without any distinct variation from cores to rims. Chondrite-normalised REE plots show flat to slightly negative patterns, with Yb_N/Gd_N values ranging from 0.27-0.53. Y values range from 135-166 ppm and europium anomalies are clear, with Eu/Eu* of 0.03-0.24 (Fig. 14b).

Monazite

REE analyses for monazite from sample I06-62 show some variation that correlates with Y contents identified by the electron probe mapping (Fig 6b-g). The Y-rich (9220-11880 ppm) core domains show a spread of chondrite-normalised HREE concentrations with Gd_N of 36775-45626 and Yb_N of 782-1508 and Eu/Eu* values of 0.26-0.28 (Fig. 15a). The low-Y (2512-6110 ppm) domains are more consistent with similar Gd_N of 37233-47660 to the cores but lower and less variable Yb_N of 77-388, with the bulk of the analyses less than 130. The Eu/Eu* values for the low-Y monazite range between 0.24-0.27 (Fig. 7d). The single younger spot analysis, m16.1, with the highest Y response (22420 ppm) from mapping had the most elevate HREE contents, with a Gd_N value of 51984, Yb_N of 3413 and a lower Eu/Eu* value of 0.28 when compared to the other Y delineated domains.

6.2 Sample I06-79

Zircon

REE analyses of zircon from sample I06-79 show two distinct patterns (Fig. 14c). Oscillatory zoned zircon cores show steep positive REE trends on a chondrite-normalised plot. Yb_N/Gd_N values are 8-180, corresponding with Y values of 412-2031 ppm and Eu/Eu* of 0.03-2.10. REE patterns for the zircon rims and CL-bright new grains show consistently flat to slightly

negative patterns on a chondrite-normalised plot (Fig. 14c). Yb_N/Gd_N values are 0.20-1.77, corresponding with lower Y values of 41-245 ppm and Eu/Eu* of 0.04-0.33.

Garnet

REE analyses for garnet from in sample I06-79 show a distinct variation in core and rim compositions (Fig.14d). Chondrite-normalised REE plots show flat to slightly positive patterns, with Yb_N/Gd_N values ranging from 4.0-5.1 and corresponding Y values range from 352-382 ppm. Europium anomalies are clear with Eu/Eu* values of 0.13-0.30 (Fig. 14d). Chondrite-normalised REE plots of garnet rims show slightly negative patterns, with Yb_N/Gd_N values ranging from 0.13-0.35 and corresponding Y values of 73-136 ppm. Europium anomalies are again pronounced with Eu/Eu* of 0.10-0.21 (Fig. 14d).

Monazite

REE analyses for monazite from this sample show a spread of chondrite-normalised REE (Fig 15b) with Gd_N of 31332-52645 and Yb_N of 52-713. Y contents of 670-9300 ppm and Eu/Eu* values for monazite range between 0.15-0.29.

7. Numerical modelling of the Madurai Block

In this section we use a 1D numerical model to explore radioactive decay as a potential heat source controlling the time scale over which crustal temperatures in the Madurai Block evolved towards high temperature conditions. Heat production values relevant to the study area (Ray et al., 2003; Ray et al., 2008) are used in the modelling and the model results are compared to the metamorphic P-T-t evolution obtained from the petrology and geochronology.

Using 2D models of orogens, previous studies have demonstrated that it is possible to reach temperatures of >800 °C in the mid crust (Beaumont et al., 2001; Beaumont et al., 2004; Faccenda et al., 2008b; Gerya et al., 2014; Jamieson and Beaumont, 2011; Jamieson et al., 2004; Jamieson et al., 2010; Lexa et al., 2011; Sizova et al., 2014). Jamieson and Beaumont (2011), in particular, have highlighted how temperatures in excess of 900 °C may be achieved in the core of a large hot orogen where rocks are deeply buried for an extended period of time and are exhumed by post-orogenic thinning. In their models the lower crustal material remains buried in the orogenic core rather than being transported towards the surface over a lower crustal ramp allowing the rocks time to incubate at depth (point 5 on their fig. 4b). In the case of the Madurai Block, the geological constraints suggest that there is a significant distance from the Tanzania craton-Azania suture zone to the area of high-T metamorphism (Figs 1B & 2) and the metamorphic P-T evolution is similar for multiple localities over a large area (Figs. 1C & 3). Accordingly, we suggest that this scenario can be approximated by a 1D model of homogenous thickening, treating the crust as a vertically uniform column that is spatially removed from the system boundaries.

To model the temporal evolution of a representative pressure-temperature path in the southern Madurai Block, we solve the standard heat flow equation in one spatial dimension with terms for conduction, radiogenic heat production, erosion and partial melting:

$$\frac{\partial T}{\partial t} = \frac{1}{\rho c_{\mathrm{mod}}}\left[\frac{\partial}{\partial z}\left(k(T)\frac{\partial T}{\partial z}\right) - u\rho c_p \frac{\partial T}{\partial z} + A_{rad}\right] \qquad \text{equation 1}$$

where T is temperature, t is time, ρ is density, k is thermal conductivity, z is depth, u is the erosion (exhumation) rate, A_{rad} is radiogenic heat production, c_p is specific heat capacity and c_{mod} is a modified heat capacity which includes the effects of partial melting (Stüwe, 1995).

The upward movement of radiogenic heat production due to erosion at the surface acts to reduce the total heat production available within the crust over the course of the orogenic event. In order to replicate a potential burial and exhumation history of a rock from within a large plateau, we delay erosion for 60 Ma post thickening and then remove 35 km of crust over the next 60 Ma. All model parameter values and their units are listed in Table 1 and the schematic of the model setup is shown in Fig. 16a.

Melting reactions in crustal rocks are strongly endothermic and we use the expressions in Stüwe (1995) to quantify this buffering effect of anatexis. The heat consumed during partial melting depends on the temperature interval between the onset (T_{min}) and completion (T_{max}) of melting, the latent heat of melting (L) and a constant (α), which determines the distribution of volumetric melt fraction over the melting interval. The effects of partial melting are incorporated into the governing equations through the use of a modified heat capacity, defined as:

$$c_{mod} = c_p + L\frac{\alpha e^{\alpha T}}{e^{\alpha T_{max}} - e^{\alpha T_{min}}} \quad \text{for } T_{min} \le T \le T_{max} \qquad \text{equation 2a}$$

and

$$c_{mod} = c_p \quad \text{for } T < T_{min} \text{ or } T > T_{max} \qquad \text{equation 2b}$$

We also include the temperature dependence of both thermal conductivity (k) and specific heat capacity (c_p). For model depths within the mantle, the expression for $k(T)$ is taken from McKenzie et al. (2005) for olivine (assuming Fo_{89}), and for crustal depths we take the expression from Mottaghy et al. (2008) based on measured data from their Transalp profile. The expressions for $c_p(T)$ are derived from the same sources. We assume constant

densities for the crust and mantle, and a uniform distribution of radiogenic heat production throughout a single layer within the crust (Table 1).

We solve the heat flow equation (1) by finite differences with a constant time increment (Δt) of 0.1 My and a constant depth interval (Δz) of 0.5 km. We discretise the finite difference equations using the unconditionally stable Crank-Nicolson method, centered in time and space. The temperature dependencies of k and c_p are handled using a method similar to that in McKenzie et al. (2005), following Press et al. (1992). We employ boundary conditions of constant surface temperature (0 °C) and a constant temperature at the base of the lithosphere (1300 °C). The Moho is initially at z = 35 km and instantaneous, homogeneous thickening of the crust by a factor of two is imposed at t = 0. A time delay in the erosive removal of crustal material is fixed at 60 My.

The results of this modelling suggest that for a uniform heat production value of 3 μWm^{-3} the crust will achieve temperatures of 900 °C approximately 60 Ma after initial thickening (Fig 16b, c). Once erosion of the upper crust begins the crust at a depth of 0.9 GPa continues to heat for a further 20 Ma and then begins to cool towards 700 °C after 120 Ma. A particle that began at a depth of 0.9 GPa will remain at temperatures of >900 °C for approximately 40 Ma in this model (Fig. 16c). At depths greater than 0.8 GPa the crust is essentially isothermal with no significant increase in temperature with depth even down to depths >1.2 GPa (Fig. 16b).

8. Discussion

8.1 Metamorphic evolution

The calculated phase equilibria for the two modelled compositions produce results that are broadly consistent. Both samples record granulite-facies conditions, with all prograde matrix biotite having been consumed in the aluminous metapelite (sample I06–62) and all prograde matrix sillimanite in the subaluminous composition (sample I06–79). The results suggest peak pressures of around 0.6–0.9 GPa at temperatures of >850 °C in sample I06–62 and close to 850 °C in sample I06–79. The presence of sillimanite inclusions in garnet and lack of evidence for the former presence of kyanite suggests the trajectory of the prograde path did not occur at pressures significantly higher than those recorded at the peak. The late growth of cordierite replacing garnet in both samples suggests they followed a clockwise path, broadly consistent with previous studies (Fig. 3; Braun et al., 2007; Brown and Raith, 1996; Mohan and Windley, 1993; Raith et al., 1997; Sajeev et al., 2001, 2004; Sajeev et al., 2006; Santosh and Kusky, 2010; Tateishi et al., 2004; Tsunogae and Santosh, 2010a, b). Although example *P*–*T* paths consistent with petrographic observations are shown on Figs 10 and 11, there are no clear constraints on their precise shape except that the rocks underwent high-*T* decompression.

8.2 Monazite growth and the timing of peak metamorphism

In sample I06-62 the apparent textural equilibrium of low-Y and HREE depleted monazite with garnet and ilmenite is consistent with monazite growth at peak conditions of >850 °C, within the garnet–ilmenite–plagioclase–sillimanite field (Fig. 10). This suggests that the age obtained from monazite likely constrains the timing of peak metamorphism. An age of 559 ± 4 Ma (Fig. 13a) was obtained from the analysis of the low-Y monazite. These relatively low-Y contents also suggest that monazite grew in equilibrium with phases that are likely to sequester Y, such as garnet. The higher-Y, elevated HREE monazite was observed as cores to

the lower Y monazite, with analyses from these domains giving ages >650 Ma (Fig. 13a), interpreted as monazite inherited from the protolith. A second high-Y, HREE-enriched monazite forms narrow rims on the low-Y monazite, and is interpreted to have grown via the retrograde breakdown of garnet. One analysis (m16.1) from the high Y rim gave a younger age of 508 ± 16 Ma (Fig. 6g; Fig. 13a; Table S1).

In sample I06-79 there was no observed correlation between the variations in the HREE geochemistry of monazite and the age obtained via SHRIMP. The textural positions of the analysed monazites, one inclusion in garnet and the other intergrown with ilmenite, are again suggestive of monazite growing on the prograde to peak portion of the *P–T* evolution at 550 ± 7 Ma. This age overlaps with that obtained from sample I06-62.

8.4 Timing and mechanisms of metamorphic zircon growth

In sample I06-62 zircon occurs in a number of different textural positions including: (1) in cordierite that forms coronas around garnet (Fig. 5a); (2) as inclusions in late biotite (Fig. 5b) and; (3) as an overgrowth on ilmenite (Fig. 5b). These textural associations imply that zircon growth was relatively late in the metamorphic history of this rock. The growth of zircon can be attributed to a number of reactions that have previously been described in high-grade metamorphic rocks. Zircon within the cordierite corona is interpreted to be the result of the breakdown of garnet during decompression. This is consistent with the flat HREE profiles for both garnet and zircon in this textural position, indicating that the two minerals were in chemical communication during the growth of zircon (e.g. Rubatto et al., 2000; Taylor et al., 2014). Fraser et al. (1997) have suggested that the release of zirconium held in garnet during garnet breakdown may result in the growth of new metamorphic zircon. Kelsey et al.

(2008) demonstrated that zircon growth is likely to occur during the crystallisation of melt and zircon overgrowths on ilmenite have previously been reported from the Norwegian Caledonides (Bingen et al., 2001), where the breakdown of ilmenite releases Zr. The lack of consistency of between the REE patterns for zircons in different textural locations suggests that the length scale of equilibration for REE is less than the scale of a single thin section in this sample. The zircon analysed in this study yields an age of 518 ± 4 Ma (n=12, MSWD=0.95 Fig. 13b). This age is within error of the single younger monazite age from the high-Y, HREE-depleted rim described above, suggesting the development of the high-Y rims on monazite and the growth of zircon were contemporaneous.

The growth of zircon from the breakdown of garnet to produce cordierite is consistent with the textural observation of zircon occurring in the cordierite corona. The zirconium released during garnet breakdown would not have been consumed by the melt because the predicted volume of melt in the rock along this segment of the *P*–*T* evolution begins to decrease (Fig. 10). As temperature decreases a potential maximum 950°C to below the solidus all of the remaining melt in the rock will crystallise promoting zircon growth, as there are no other phases able to incorporate the zirconium being released.

In sample I06-79 the HREE patterns are consistent with zircon rims and CL-bright whole grains having grown in equilibrium with garnet rims (Fig. 8c, d). Zircon textures in this sample are similar to those that have been demonstrated to have grown from crystallising melts (Hoskin and Black, 2000; Vavra et al., 1996). This reinforces the notion that zircon records both the timing of the breakdown of garnet during decompression and cooling and crystallisation of the melt that remained in the rocks after peak temperature conditions had been reached. The U-Pb age of 512 ± 4 Ma obtained from the zircon from this sample is within analytical uncertainty of the zircon age from I06-62.

A further outcome of the SHRIMP U-Pb study is revealed by the spectrum of ages from the analysed zircon cores. Concordant U-Pb ages ranging from 2640 Ma to 686 Ma suggest that the protoliths to the metasedimentary rocks in the southern Madurai Block were deposited in the Neoproterozoic. This is consistent with recent studies of the zircon U-Pb systematics of protoliths that have identified this block as comprising a suite of younger sediments that were deposited in the Mozambique Ocean prior to the collision of Greater India with East Africa (Collins et al., 2014; Plavsa et al., 2012; Plavsa et al., 2014; Teale et al., 2012).

8.5 What drove high temperature metamorphism in the Madurai Block?

There have been numerous studies that deal with the thermal structure of the lithosphere during orogenesis (Beaumont et al., 2010; Beaumont et al., 2001; Beaumont et al., 2004; Depine et al., 2008; England and Molnar, 1993; England and Richardson, 1977; England and Thompson, 1984; Jamieson and Beaumont, 1988; Jamieson et al., 2004; Jamieson et al., 2010; Lachenbruch, 1970), and some that have focussed on the extent to which enrichment in HPE in the crust can lead to elevated temperatures in the mid-crust (Chamberlain and Sonder, 1990; England and Thompson, 1984; Faccenda et al., 2008a; Goffe et al., 2003; Huerta et al., 1998; Le Pichon et al., 1997; Sandiford and Hand, 1998). More recent numerical modelling of orogens have produced results that suggest if the crust is significantly enriched in HPE and deeply buried (Lexa et al., 2011), if crustal material with moderate HPE levels is kept at depth for a long period of time (Jamieson and Beaumont, 2011; Jamieson et al., 2010; McKenzie and Priestley, 2008) or there is significant addition of heat input from the deformation of strong lithologies (Nabelek et al., 2010) then the crust may be able to be heated to temperatures in excess of 900 °C at depths consistent with observations from UHT metamorphic terranes. In

the previous sections we have constrained the *P*–*T*–*t* history of one such occurrence from the SGT in India.

In the specific case of the SGT the petrological and geochronological data suggest that temperatures required for the crust to start melting (~700 °C) would have been achieved within 20 My of thickening, a duration that is consistent with constraints from the Himalayas that suggest that melting began within 25 My of the onset of crustal thickening (Harris et al., 1995; Harris et al., 2000; Harris et al., 2004). As crustal temperatures continued to rise, UHT metamorphic conditions were achieved at ~560 Ma, approximately 60 My after the proposed collision of the Azania microcontinent with East Africa. This duration is consistent with the results from our 1–D numerical modelling for the time needed for moderately enriched crust to conductively heat to granulite-facies temperatures. This can be seen in Fig. 16c, where the *P*–*T* path for a particle that starts at 0.9 GPa intersects the peak fields as constrained by the pseudosection modelling after 60 Ma (Fig. 16c). However, it should be noted that the intergrowth of monazite and garnet occurs over a range of temperatures that cannot adequately be described by a single age population, and it may be more appropriate to consider the growth of monazite to have occurred over a broader time interval than the reported error on the age indicates. One could consider this time interval to be broadly constrained by the range of individual spot ages that, in this case, range between 575 to 540 Ma (Fig. 13a, c). In addition, it should also be acknowledged that 575 Ma is a minimum estimate for the upper age limit as at such high temperatures there may be a degree of Pb-loss and partial resetting of monazite along the concordia that is unresolvable with current techniques (Korhonen et al., 2013; Mezger and Krogstad, 1997).

The growth of zircon triggered by the breakdown of garnet and ilmenite and the crystallisation of melt at temperatures in excess of around 900°C at 518 Ma indicates that the crustal rocks in the SGT remained at temperatures in excess of 900°C for over 40 My. The

range of ages in this study, when linked to the petrological development of the silicate assemblages via REE geochemistry from the two investigated samples, is consistent with a long-lived heat source. Given the absence of any coincident large-volume magmatic rocks in the SGT, an alternative to magmatic heating must be found. The dataset of Ray et al. (2003) demonstrates that there are large volumes of rock within the SGT that have average heat production values of greater than 3 μWm^{-3} at 550 Ma, and we propose this as a plausible long-lived heat source for metamorphism in the SGT.

8.6 Implications for the formation of regional scale granulite and UHT metamorphic terranes through Earth history

In the previous discussion it is suggested that the major contributor to the generation of regional scale UHT conditions in the SGT is the heat produced due to the decay of HPEs in thickened crust. A good starting point to test the applicability of this mechanism to the generation of granulite and UHT (G-UHT) terranes through time is to see how it can be related to the observation that G-UHT metamorphism is cyclical in nature, and that there is a first order link between the supercontinent cycle and the generation and preservation of regional scale G-UHT terranes (Brown, 2006). For our model to be appropriate to the generation of G-UHT conditions in other G-UHT terranes throughout Earth history, a number of conditions must be satisfied.

The primary requirement for radiogenic heat production to be the heat source for the generation of regional-scale G-UHT metamorphic conditions is that there is the requisite concentration of HPEs in the crustal column. The observed link between the occurrence of G-UHT conditions and the terminal stages of supercontinent amalgamation may provide a mechanism for the enrichment of the crustal column in HPEs. It has been proposed that

continents reorganize by two contrasting processes, known as extroversion or introversion, or by a combination of both (Murphy and Nance, 2003, 2013; Murphy et al., 2009). Extroversion, is where a supercontinent rifts apart and then turns inside-out to form a second supercontinent along suture zones that correspond to the margins of the first supercontinent. In contrast, introversion, is where the first supercontinent rifts apart forming an internal ocean and then reassembles through the closure of the newly created ocean forming a second supercontinent. The process of extroversion, which is interpreted to be the driving mechanism for the formation and destruction of several past supercontinents in Earth history such as Vaalbara, Columbia, Rodinia and Gondwana (Murphy and Nance, 2013; Nance et al., 2014), would have resulted in the development of large passive margins of material derived from the erosive removal of the collisional mountain systems formed during continental collision. The reworking and redistribution of HPE within these collisional orogens, and their erosion and deposition at the margins of a supercontinent where they can be incorporated into the next supercontinent cycle, provides a mechanism for the heat source for the generation of regional scale G-UHT terranes. However, these ideas need to be tested in more detail through studies integrating geochronological and petrological data that focus on the duration and *P*–*T* conditions of metamorphism in each of these terranes.

Secondly, as partial melting acts as a heat sink during the evolution of a terrane to high temperatures, a requirement for a terrane to attain G-UHT conditions, effectively evolving from a regional scale migmatite terrane into a G-UHT terrane, is that the duration of orogenesis must be long enough (>60 Ma for average crustal heat productions of 3 μW^{-3}) for the radiogenic heat source to provide the required thermal energy to overcome the thermal buffering effect of partial melting (e.g. Clark et al., 2011). This means that the orogen must be either large in scale or that erosion rates are slow enough to retard the removal of the HPEs. The observation by Brown (Brown, 2006, 2007) that the age distribution of metamorphic

belts that record regional scale G-UHT metamorphism is not uniform and can be broadly correlated with the amalgamation of the continental lithosphere into supercratons or supercontinents is suggestive of a correlation between the two processes. Whereas Brown (Brown, 2006) suggests that G-UHT metamorphism is related to the generation of initially high geothermal gradient conditions in continental back-arc regions prior to crustal thickening, we propose that G-UHT conditions actually relate to the final stage of amalgamation (i.e. continent–continent collision). The thickening of the crust during continental collision during the amalgamation of Gondwana has been likened to the generation of a Himalayan-scale continental collision system (Santosh et al., 2009). This correlation between the terminal phase of collision during supercontinent amalgamation fulfils the requirement that a long-lived collisional system is integral to the cyclic generation of regional scale G-UHT conditions in nature.

While the scenario related to the formation and reorganisation of supercontinents described above fulfils a number of criteria in regard to the apparent cyclicity of G-UHT terranes it should also be noted that continental margins and other thick sedimentary basins on thinned crust and lithosphere, including continental backarcs, are naturally enriched in HPE. Any collision involving a rifted continental margin, or closure of a continental back-arc basin, will result in thickened HPE-enriched sections and lead to the development of elevated geothermal gradients. Provided the crust remains thickened for long enough, there is the potential for the achievement of G-UHT conditions in any orogenic system of this type.

Acknowledgements

We thank Michael Brown and Brad Hacker from the Journal for their constructive comments. We are particularly grateful to Rebecca Jamieson whose detailed review led to significant

improvements in the manuscript. Kevin Blake at James Cook University is thanked for assistance in the use of the electron microprobe. CC and RT acknowledge support from Curtin University Strategic Research Funding. Funding for analyses and fieldwork was provided through Australian Research Council Discovery and DECRA projects DP0879330 and DE1201030 and Australia-India Strategic Research Fund project #ST030046. Zircon and monazite U-Pb analyses were carried out using the SHRIMP-II Ion Microprobe at the John de Laeter Centre for Isotope Research, Perth, managed by Allen Kennedy on behalf of a consortium consisting of Curtin University, the Geological Survey of Western Australia, and the University of Western Australia with the support of the Australian Research Council. REE analyses were carried out at the LA-ICP-MS Facility at the Dept. of Applied Geology at Curtin University. ASC acknowledges funding from the Australian Research Council Future Fellowship Scheme # FT120100340. ASC's contribution forms TRaX Record #306.

References

Bartlett, J.M., Dougherty-Page, J.S., Harris, N.B.W., Hawkesworth, C.J., Santosh, M., 1998. The application of single zircon evaporation and model Nd ages to the interpretation of polymetamorphic terrains: an example from the Proterozoic mobile belt of south India. Contributions to Mineralogy and Petrology 131, 181-195.

Beaumont, C., Jamieson, R., Nguyen, M., 2010. Models of large, hot orogens containing a collage of reworked and accreted terranes. Canadian Journal of Earth Sciences 47, 485-515.

Beaumont, C., Jamieson, R.A., Nguyen, M.H., Lee, B., 2001. Himalayan tectonics explained by extrusion of a low-viscosity crustal channel coupled to focused surface denudation. Nature 414, 738-742.

Beaumont, C., Jamieson, R.A., Nguyen, M.H., Medvedev, S., 2004. Crustal channel flows: 1. Numerical models with applications to the tectonics of the Himalayan-Tibetan orogen. Journal of Geophysical Research-Solid Earth 109.

Bhaskar Rao, Y.J., Janardhan, A.S., Vijaya Kumar, T., Narayana, B.L., Dayal, A.M., Taylor, P.N., Chetty, T.R.K., 2003. Sm-Nd model ages and Rb-Sr isotope systematics of charnockites and gneisses across the Cauvery Shear Zone, southern India: implications for the Archaean-Neoproterozoic boundary in the southern granulite terrain, In: Ranmakrishnan, M. (Ed.), Tectonics of Southern Granulite Terrain. Geological Society of India Memoir 50, pp. 297-317.

Bingen, B., Austrheim, H., Whitehouse, M., 2001. Ilmenite as a source for zirconium during high-grade metamorphism? Textural evidence from the Caledonides of western Norway and implications for zircon geochronology. Journal of Petrology 42, 355-375.

Boger, S.D., Hirdes, W., Ferreira, C.A.M., Schulte, B., Jenett, T., Fanning, C.M., 2014. From passive margin to volcano–sedimentary forearc: The Tonian to Cryogenian evolution of the Anosyen Domain of southeastern Madagascar. Precambrian Research 247, 159-186.

Brandt, S., Raith, M.M., Schenk, V., Sengupta, P., Srikantappa, C., Gerdes, A., 2014. Crustal evolution of the Southern Granulite Terrane, south India: New geochronological and geochemical data for felsic orthogneisses and granites. Precambrian Research 246, 91-122.

Brandt, S., Schenk, V., Raith, M.M., Appel, P., Gerdes, A., Srikantappa, C., 2011. Late Neoproterozoic P-T evolution of HP-UHT Granulites from the Palni Hills (South India): New Constraints from Phase Diagram Modelling, LA-ICP-MS Zircon Dating and in-situ EMP Monazite Dating. Journal of Petrology 52, 1813-1856.

Braun, I., Cenki-Tok, B., Paquette, J.L., Tiepolo, M., 2007. Petrology and U-Th-Pb geochronology of the sapphirine-quartz-bearing metapelites from Rajapalayam, Madurai Block, Southern India: Evidence for polyphase Neoproterozoic high-grade metamorphism. Chemical Geology 241, 129-147.

Braun, I., Raith, M., Ravindra Kumar, G.R., 1996. Dehydration-melting phenomena in leptynitic gneisses and the generation of leucogranites: a case study from the Kerala Khondalite Belt, southern India. Journal of Petrology 37, 1285-1305.

Brown, M., 2006. Duality of thermal regimes is the distinctive characteristic of plate tectonics since the Neoarchean. Geology 34, 961-964.

Brown, M., 2007. Metamorphic conditions in orogenic belts: A record of secular change. International Geology Review 49, 193-234.

Brown, M., Raith, M., 1996. First evidence of ultrahigh-temperature decompression from the granulite province of southern India. Journal of the Geological Society 153, 819-822.

Buick, I.S., Clark, C., Rubatto, D., Hermann, J., Pandit, M., Hand, M., 2010. Constraints on the Proterozoic evolution of the Aravalli-Delhi Orogenic belt (NW India) from monazite geochronology and mineral trace element geochemistry. Lithos 120, 511-528.

Cawood, P.A., Buchan, C., 2007. Linking accretionary orogenesis with supercontinent assembly. Earth Science Reviews 85, 217-256.

Chamberlain, C.P., Sonder, L.J., 1990. Heat-producing elements and the thermal and baric patterns of metamorphic belts. Science 250, 763-769.

Clark, C., Collins, A.S., Santosh, M., Taylor, R., Wade, B.P., 2009a. The P-T-t architecture of a Gondwanan suture: REE, U-Pb and Ti-in-zircon thermometric constraints from the Palghat Cauvery shear system, South India. Precambrian Research 174, 129-144.

Clark, C., Collins, A.S., Timms, N.E., Kinny, P.D., Chetty, T.R.K., Santosh, M., 2009b. SHRIMP U-Pb age constraints on magmatism and high-grade metamorphism in the Salem Block, southern India. Gondwana Research 16, 27-36.

Clark, C., Fitzsimons, I.C.W., Healy, D., Harley, S.L., 2011. How does the continental crust get really hot? Elements 7, 233-238.

Clark, C., Kirkland, C.L., Spaggiari, C.V., Oorschot, C., Wingate, M.T.D., Taylor, R.J., 2014. Proterozoic granulite formation driven by mafic magmatism: An example from the Fraser Range Metamorphics, Western Australia. Precambrian Research 240, 1-21.

Collins, A.S., 2006. Madagascar and the amalgamation of Central Gondwana. Gondwana Research 9, 3-16.

Collins, A.S., Clark, C., Plavsa, D., 2014. Peninsular India in Gondwana: The tectonothermal evolution of the Southern Granulite Terrain and its Gondwanan counterparts. Gondwana Research 25, 190-203.

Collins, A.S., Clark, C., Sajeev, K., Santosh, M., Kelsey, D.E., Hand, M., 2007a. Passage through India: the Mozambique Ocean suture, high-pressure granulites and the Palghat-Cauvery shear zone system. Terra Nova 19, 141-147.

Collins, A.S., Clark, C., Santosh, M., Chetty, T.R.K., 2008. Ediacaran-Cambrian tectonic evolution of southern India. The Indian Journal of Geology 80, 23-40.

Collins, A.S., Fitzsimons, I.C.W., Hulscher, B., Razakamanana, T., 2003. Structure of the eastern margin of the East African Orogen in central Madagascar. Precambrian Research 123, 111-133.

Collins, A.S., Kinny, P.D., Razakamanana, T., 2012. Depositional age, provenance and metamorphic age of metasedimentary rocks from southern Madagascar. Gondwana Research 21, 353-361.

Collins, A.S., Pisarevsky, S.A., 2005. Amalgamating eastern Gondwana: The evolution of the Circum-Indian Orogens. Earth-Science Reviews 71, 229-270.

Collins, A.S., Santosh, M., Braun, I., Clark, C., 2007b. Age and sedimentary provenance of the Southern Granulites, South India: U-Th-PbSHRIMP secondary ion mass spectrometry. Precambrian Research 155, 125-138.

Compston, W., Williams, I.S., Meyer, C., 1984. U-Pb geochronology of zircons from lunar breccia 73217 using a sensitive high mass-resolution ion microprobe. Proceedings of the 14th Lunar and Planetary Science Conference Part 2. Journal of Geophysical Research 89 (Supplement), B525-B534.

de Wit, M.J., Bowring, S.A., Ashwal, L.D., Randrianasolo, L.G., Morel, V.P.I., Rambeloson, R.A., 2001. Age and Tectonic Evolution of Neoproterozoic ductile shear zones in southwestern Madagascar, with implications for Gondwana studies. Tectonics 20, 1-45.

Degeling, H., Eggins, S., Ellis, D.J., 2001. Zr budgets for metamorphic reactions, and the formation of zircon from garnet breakdown. Mineralogical Magazine 65, 749-758.

Depine, G.V., Andronicos, C.L., Phipps-Morgan, J., 2008. Near-isothermal conditions in the middle and lower crust induced by melt migration. Nature 452, 80-83.

Emmel, B., Jons, N., Kroner, A., Jacobs, J., Wartho, J.A., Schenk, V., Razakamanana, T., Austegard, A., 2008. From closure of the Mozambique Ocean to Gondwana breakup: New evidence from geochronological data of the Vohibory terrane, southwest Madagascar. Journal of Geology 116, 21-38.

England, P., Molnar, P., 1993. The interpretation of inverted metamorphic isograds using simple physical calculations. Tectonics 12, 145-157.

England, P., Richardson, S.W., 1977. The influence of erosion upon the mineral facies of rocks from different metamorphic environments. Journal of the Geological Society of London 134, 201-213.

England, P.C., Thompson, A.B., 1984. Pressure-temperature time paths of regional metamorphism. Heat transfer during the evolution of thickening continental crust. Journal of Petrology 25, 894-928.

Faccenda, M., Gerya, T.V., Burlini, L., Chakraborty, S., 2008a. Numerical modelling of continental collision, oceanic subduction and related geodynamical processes. Geochimica Et Cosmochimica Acta 72, A250-A250.

Faccenda, M., Gerya, T.V., Chakraborty, S., 2008b. Styles of post-subduction collisional orogeny: Influence of convergence velocity, crustal rheology and radiogenic heat production. Lithos 103, 257-287.

Fitzsimons, I.C.W., Hulscher, B., 2005. Out of Africa: detrital zircon provenance of central Madagascar and Neoproterozoic terrane transfer across the Mozambique Ocean. Terra Nova 17, 224-235.

Foster, G., Kinny, P., Vance, D., Prince, C., Harris, N., 2000. The significance of monazite U-Th-Pb age data in metamorphic assemblages; a combined study of monazite and garnet chronometry. Earth and Planetary Science Letters 181, 327-340.

Fraser, G., Ellis, D., Eggins, S., 1997. Zirconium abundance in granulite-facies minerals, with implications for zircon geochronology in high-grade rocks. Geology 27, 607-610.

Gerya, T., Santosh, M., Slabunov, A., Safonova, I., 2014. Granulites and eclogites in geodynamics: Preface. Gondwana Research 25, 439-441.

Gerya, T.V., Meilick, F.I., 2011. Geodynamic regimes of subduction under an active margin: effects of rheological weakening by fluids and melts. Journal of Metamorphic Geology 29, 7-31.

Goffe, B., Bousquet, R., Henry, P., Le Pichon, X., 2003. Effect of the chemical composition of the crust on the metamorphic evolution of orogenic wedges. Journal of Metamorphic Geology 21, 123-141.

Hacker, B.R., Gnos, E., Ratschbacher, L., Grove, M., McWilliams, M., Sobolev, S.V., Wan, J., Zhenhan, W., 2000. Hot and dry deep crustal xenoliths from Tibet. Science 287, 2463-2466.

Harris, N., Ayres, M., Massey, J., 1995. Geochemistry of granitic melts produced during the incongruent melting of muscovite: implications for the extraction of Himalayan leucogranite magmas. J Geophys Res 100, 15,767-715,777.

Harris, N., Vance, D., Ayres, M., 2000. From sediment to granite: Timescales of anatexis in the upper crust. Chem Geol 162, 155-167.

Harris, N.B.W., Caddick, M., Kosler, J., Goswami, S., Vance, D., Tindle, A.G., 2004. The pressure-temperature-time path of migmatites from the Sikkim Himalaya. Journal of Metamorphic Geology 22, 249-264.

Hinthorne, J.R., Anderson, C.A., Conrad, R.L., Lovering, J.F., 1979. Single-grain 207Pb/206Pb and U/Pb age determinations with a 10 μm spatial resolution using the ion microprobe mass analyser (IMMA). Chemical Geology 25, 271-303.

Holland, T.J.B., Powell, R., 2011. An improved and extended internally consistent thermodynamic dataset for phases of petrological interest, involving a new equation of state for solids. Journal of Metamorphic Geology 29, 333-383.

Hoskin, P.W.O., Black, L.P., 2000. Metamorphic zircon formation by solid-state recrystallization of protolith igneous zircon. Journal of Metamorphic Geology 18, 423-439.

Huerta, A.D., Royden, L.H., Hodges, K.V., 1998. The thermal structure of collisional orogens as a response to accretion, erosion, and radiogenic heating. Journal of Geophysical Research 103, 15287-15302.

Jamieson, R.A., Beaumont, C., 1988. Orogeny and metamorphism: a model for deformation and pressure-temperature-time paths with applications to the central and southern Appalachians Tectonics 7, 417-445.

Jamieson, R.A., Beaumont, C., 2011. Coeval thrusting and extension during lower crustal ductile flow - implications for exhumation of high-grade metamorphic rocks. Journal of Metamorphic Geology 29, 33-51.

Jamieson, R.A., Beaumont, C., Medvedev, S., Nguyen, M.H., 2004. Crustal channel flows: 2. Numerical models with implications for metamorphism in the Himalayan-Tibetan orogen. Journal of Geophysical Research-Solid Earth 109.

Jamieson, R.A., Beaumont, C., Warren, C.J., Nguyen, M.H., 2010. The Grenville Orogen explained? Applications and limitations of integrating numerical models with geological and geophysical data. Canadian Journal of Earth Sciences 47, 517-539.

Jayananda, M., Janardhan, A.S., Sivasubramanian, P., Peucat, J.J., 1995. Geochronological and isotopic constraints on granulite formation in the Kodiakanal area, southern India. Geological Society of India, Memoir 34, pp. 373-390.

Jöns, N., Schenk, V., 2008. Relics of the Mozambique Ocean in the central East African Orogen: evidence from the Vohibory Block of southern Madagascar. Journal of Metamorphic Geology 26, 17-28.

Kelly, N.M., Harley, S.L., 2005. An integrated microtextural and chemical approach to zircon geochronology: refining the Archaean history of the Napier Complex, east Antarctica. Contributions to Mineralogy and Petrology 149, 57-84.

Kelsey, D.E., Clark, C., Hand, M., 2008. Thermobarometric modelling of zircon and monazite growth in melt-bearing systems: examples using model metapelitic and metapsammitic granulites. Journal of Metamorphic Geology 26, 199-212.

Kelsey, D.E., Clark, C., Hand, M., Collins, A.S., 2006. Comment on "First report of garnet-corundum rocks from southern India: Implications for prograde high-pressure (eclogite-facies?) metamorphism". Earth and Planetary Science Letters 249, 529-534.

Kelsey, D.E., Hand, M., Clark, C., Wilson, C.J.L., 2007. On the application of in situ monazite chemical geochronology to constraining P-T-t histories in high-temperature (>850 ∞C) polymetamorphic granulites from Prydz Bay, East Antarctica. Journal of the Geological Society 164, 667-683.

Kondou, N., Tsunogae, T., Santosh, M., Shimizu, H., 2009. Sapphirine plus quartz assemblage from Ganguvarpatti: diagnostic evidence for ultrahigh-temperature metamorphism in central Madurai Block, southern India. Journal of Mineralogical and Petrological Sciences 104, 285-289.

Korhonen, F.J., Clark, C., MBrown, M., Bhattacharya, S., Taylor, R., 2013. How long-lived is ultrahigh temperature (UHT) metamorphism? Constraints from zircon and monazite geochronology in the Eastern Ghats orogenic belt, India. Precambrian Research 234, 322-350.

Korhonen, F.J., Saw, A.K., Clark, C., Brown, M., Bhattacharya, S., 2011. New constraints on UHT metamorphism in the Eastern Ghats Province through the application of phase equilibria modelling and in situ geochronology. Gondwana Research 20, 764-781.

Lachenbruch, A.H., 1970. Crustal temperature and heat production: Implications of the linear heat-flow relation. Journal of Geophysical Research 75, 3291-3300.

Le Pichon, X., Henry, P., Goffe, B., 1997. Uplift of Tibet: from eclogites to granulites-implications for the Andean Plateau and Variscan belt. Tectonophysics 273, 57-76.

Lexa, O., Schulmann, K., Janousek, V., Stipska, P., Guy, A., Racek, M., 2011. Heat sources and trigger mechanisms of exhumation of HP granulites in Variscan orogenic root. Journal of Metamorphic Geology 29, 79-102.

Ludwig, K.R., 2001. User's guide to SQUID 2. Berkeley Geochronology Center, Berkeley, p. 90.

Ludwig, K.R., 2003. Users Manual for Isoplot/Ex, Version 3.00, A Geochronological Toolkit for Microsoft Excel. Berkeley Geochronology Centre, Berkeley, CA, 2003. Special Publication No.4.

McKenzie, D., Jackson, J., Priestley, K., 2005. Thermal structure of oceanic and continental lithosphere. Earth and Planetary Science Letters 233, 337-349.

McKenzie, D., Priestley, K., 2008. The influence of lithospheric thickness variations on continental evolution. Lithos 102, 1-11.

Meert, J.G., Nédélec, A., Hall, C., 2003. The stratoid granites of central Madagascar: paleomagnetism and further age constraints on Neoproterozoic deformation. Precambrian Research 120, 101-129.

Mezger, K., Krogstad, E.J., 1997. Interpretation of discordant U-Pb zircon ages: An evaluation. Journal of Metamorphic Geology 15, 127-140.

Mohan, A., Windley, B.F., 1993. Crustal Trajectory of Sapphirine-Bearing Granulites from Ganguvarpatti, South-India - Evidence for an Isothermal Decompression Path. Journal of Metamorphic Geology 11, 867-878.

Möller, A., K., M., Schenk, V., 2000. U-Pb dating of metamorphic minerals: Pan-African metamorphism and prolonged slow cooling of high pressure granulites in Tanzania East Africa. Precambrian Research 104, 123-145.

Möller, A., Mezger, K., Schenk, V., 1998. Crustal age domains and the evolution of the continental crust in the Mozambique belt of Tanzania: combined Sm-Nd, Rb-Sr, and Pb-Pb isotopic evidence. Journal of Petrology 39, 749-783.

Morimoto, T., Santosh, M., Tsunogae, T., Yoshimura, Y., 2004. Spinel+quartz association from the Keral khondalites, southern India: evidence for ultrahigh-temperature metamorphism. Journal of Mineralogical and Petrological Sciences 99, 257-278.

Mottaghy, D., Vosteen, H.D., Schellschmidt, R., 2008. Temperature dependence of the relationship of thermal diffusivity versus thermal conductivity for crystalline rocks. International Journal of Earth Sciences 97, 435-442.

Murphy, J.B., Nance, R.D., 2003. Do supercontinents introvert or extrovert?: Sm-Nd isotope evidence. Geology 31, 873-876.

Murphy, J.B., Nance, R.D., 2013. Speculations on the mechanisms for the formation and breakup of supercontinents. . Geoscience Frontiers 4, 185-194.

Murphy, J.B., Nance, R.D., Cawood, P.A., 2009. Contrasting modes of superconinent formation and the conundrum of Pangea. . Gondwana Research 15, 408-420.

Nabelek, P.I., Whttington, A.G., Hofmeister, A.M., 2010. Strain-heating as a mechanism for partial melting and UHT metamorphism in convergent orogens: Implicatins of temperature-dependent thermal diffusivity and rheology. Journal of Geophysical Research 115, B12417.

Nance, R.D., Murphy, J.B., Santosh, M., 2014. The supercontinent cycle: A retrospective essay. Gondwana Research 25, 4-29.

Nandakumar, V., Harley, S.L., 2000. A reappraisal of the pressure-temperature path of granulites from the Kerala Khondalite Belt, Southern India. Journal of Geology 108, 687-703.

Nedelec, A., Stephens, W.E., Fallick, A.E., 1995. The Panafrican Stratoid Granites of Madagascar - Alkaline Magmatism in a Post Collisional Extensional Setting. Journal of Petrology 36, 1367-1391.

Nishimiya, Y., Tsunogae, T., Santosh, M., 2010. Sapphirine plus quartz corona around magnesian (X-Mg similar to 0.58) staurolite from the Palghat-Cauvery Suture Zone, southern India: Evidence for high-pressure and ultrahigh-temperature metamorphism within the Gondwana suture. Lithos 114, 490-502.

Plavsa, D., Collins, A.S., Foden, J.F., Kropinski, L., Santosh, M., Chetty, T.R.K., Clark, C., 2012. Delineating crustal domains in Peninsular India: Age and chemistry of orthopyroxene-bearing felsic gneisses in the Madurai Block. Precambrian Research 198, 77-93.

Plavsa, D., Collins, A.S., Payne, J.L., Foden, J.F., Clark, C., Santosh, M., 2014. Detrital zircons in basement metasedimentary protoliths unveil the origins of southern India. GSA Bulletin 126, 791-811.

Press, W.H., Teukolsky, S.A., Vetterling, W.T., Flannery, B.P., 1992. Numerical Recipes. Cambridge University Press.

Raith, M., Karmakar, S., Brown, M., 1997. Ultra-high-temperature metamorphism and multistage decompressional evolution of sapphirine granulites from the Palni Hill Ranges, southern India. Journal of Metamorphic Geology 15, 379-399.

Ray, L., Kumar, S., Reddy, G.K., Roy, S., Rao, G.V., Srinivasan, R., Rao, R.U.M., 2003. High mantle heat flow in a Precambrian granulite province: Evidence from southern India. Journal of Geophysical Research-Solid Earth 108.

Ray, L., Roy, S., Srinivasan, R., 2008. High radiogenic heat production in the Kerala Khondalite Block, Southern Granulite Province, India. International Journal of Earth Sciences 97, 257-267.

Reeves, C.V., Sahu, B.K., De Wit, M.J., 2002. A re-examination of the paleo-position of Africa's eastern neighbours in Gondwana. Journal of African Earth Sciences 34, 101-108.

Sajeev, K., Osanai, Y., Santosh, M., 2001. Ultrahigh-temperature stability of sapphirine and kornerupine in Ganguvarpatti granulite, Madurai Block, southern India. Gondwana Research 4, 762-766.

Sajeev, K., Osanai, Y., Santosh, M., 2004. Ultrahigh-temperature metamorphism followed by two-stage decompression of garnet-orthopyroxene-sillimanite granulites from Ganguvarpatti, Madurai block, southern India. Contributions to Mineralogy and Petrology 148, 29-46.

Sajeev, K., Santosh, M., Kim, H.S., 2006. Partial melting and P-T evolution of the Kodaikanal Metapelite Belt, southern India. Lithos 92, 465-483.

Sajeev, K., Windley, B.F., Connolly, J.A.D., Kon, Y., 2009. Retrogressed eclogite (20 kbar, 1020 °C) from the Neoproterozoic Palghat-Cauvery suture zone, southern India. Precambrian Res 171, 23-36.

Sandiford, M., Hand, M., 1998. Australian Proterozoic high-temperature, low-pressure metamorphism in the conductive limit, In: Treloar, P.J., O'Brien, P.J. (Eds.), What Drives Metamorphism and Metamorphic Reactions? Geological Society of London, pp. 109-120.

Santosh, M., Collins, A.S., Tamashiro, I., Koshimoto, S., Tsutsumi, Y., Yokoyama, K., 2006. The timing of ultrahigh-temperature metamorphism in Southern India: U-Th-Pb electron microprobe ages from zircon and monazite in sapphirine-bearing granulites. Gondwana Research 10, 128-155.

Santosh, M., Kusky, T., 2010. Origin of paired high pressure-ultrahigh-temperature orogens: A ridge subduction and slab window model. Terra Nova 22, 35-42.

Santosh, M., Maruyama, S., Sato, K., 2009. Anatomy of a Cambrian suture in Gondwana: Pacific-type orogeny in southern India? . Gondwana Research 16, 321-341.

Santosh, M., Rajesh, V.J., Tsunogae, T., Arai, S., 2010. Diopsidites from a Neoproterozoic-Cambrian suture in southern India. Geological Magazine 147, 777-788.

Santosh, M., Xiao, W.J., Tsunogae, T., Chetty, T.R.K., Yellappa, T., 2012. The Neoproterozoic subduction complex in southern India: SIMS zircon U–Pb ages and implications for Gondwana assembly. . Precambrian Research 192-195, 190-208.

Santosh, M., Yokoyama, K., Biju-Sekhar, S., Rogers, J.J.W., 2003. Multiple tectonothermal events in the granulite blocks of southern India revealed from EPMA dating: Implications on the history of Supercontinents. Gondwana Research 6, 29-63.

Satish-Kumar, M., 2000. Ultrahigh-temperature metamorphism in Madurai granulites, southern India: evidence from carbon isotope thermometry. Journal of Geology 108, 479-486.

Shimpo, M., Tsunogae, T., Santosh, M., 2006. First report of garnet-corundum rocks from southern India: Implications for prograde high-pressure (eclogite-facies?) metamorphism. Earth and Planetary Science Letters 242, 111-129.

Sizova, E., Gerya, T., Brown, M., 2014. Contrasting styles of Phanerozoic and Precambrian continental collision. Gondwana Research 25, 522-545.

Stern, R., 2001. A new isotopic and trace-element standard for the ion-microprobe: preliminarythermal ionisation mass spectrometry (TIMS) U-Pb and electron microprobe data, Current Research 2001-F1. Geological Survey of Canada, pp. 1-11.

Stüwe, K., 1995. Thermal buffering effects at the solidus. Implicaitons for the equilibration of partially melted metamorphic rocks. Tectonophysics 248, 39-51.

Tadokoro, H., Tsunogae, T., Santosh, M., Yoshimura, Y., 2007. First report of the spinel plus quartz assemblage from Kodaikanal in the Madurai block, southern India: Implications for ultrahigh-temperature metamorphism. International Geology Review 49, 1050-1068.

Tateishi, K., Tsunogae, T., Santosh, M., Janardhan, A.S., 2004. First report of sapphirine plus quartz assemblage from southern India: Implications for ultrahigh-temperature metamorphism. Gondwana Research 7, 899-912.

Teale, W., Collins, A.S., Foden, J.F., Payne, J.L., Plavsa, D., Chetty, T.R.K., Santosh, M., Fanning, C.M., 2012. Cryogenian (~ 830Ma) mafic magmatism and metamorphism in the northern Madurai Block, southern India: A magmatic link between Sri Lanka and Madagascar? Journal of Asian Earth Sciences 42, 223-233.

Tsunogae, T., Santosh, M., 2010a. Sapphirine + quartz assemblage from the Southern Granulite Terrane, India: diagnostic evidence for ultrahigh-temperature metamorphism within the Gondwana collisional orogen. Geological Journal 46, 183-197.

Tsunogae, T., Santosh, M., 2010b. Ultrahigh-temperature metamorphism and decompression history of sapphirine granulites from Rajapalaiyam, southern India: implications for the formation of hot orogens during Gondwana assembly. Geological Magazine 147, 42-58.

Tucker, R., Roig, J., Macey, P., Delor, C., Amelin, Y., Armstrong, R., Rabarimanana, M., Ralison, A., 2011a. A new geological framework for south-central Madagascar, and its relevance to the "out-of-Africa" hypothesis. Precambrian Res 185, 109-130.

Tucker, R., Roig, J.-Y., Delor, C., Amelin, Y., Goncalves, P., Rabarimanana, M., Ralison, A., Belcher, R., 2011b. Neoproterozoic extension in the Greater Dharwar Craton: a reevaluation of the ''Betsimisaraka suture'' in Madagascar. Canadian Journal of Earth Sciences 48, 389-417.

Tucker, R.D., Roig, J.Y., Moine, B., Delor, C., Peters, S.G., 2014. A geological synthesis of the Precambrian shield in Madagascar. Journal of African Earth Sciences 94, 9-30.

Vavra, G., Gebauer, D., Schmid, R., Compston, W., 1996. Multiple zircon growth and recystallization during polyphase Late Carboniferous to Triassic metamorphism in granulites of the Ivrea Zone (Southern Alps): an ion microprobe (SHRIMP) study. Contributions to Mineralogy and Petrology 122, 337-358.

Vila, M., Fernandez, M., Jimenez-Munt, I., 2010. Radiogenic heat production variability of some common lithological groups and its significance to lithospheric thermal modeling. Tectonophysics 490, 152-164.

White, R.W., Powell, R., Holland, T.J.B., Johnson, T.E., Green, E.C.R., 2014. New mineral activity-composition relations for thermodynamic calculations in metapelitic systems. Journal of Metamorphic Geology 32, 261-286.

Yakymchuk, C., Brown, M., 2014. Behaviour of zircon and monazite during crustal melting. Journal of the Geological Society of London 171, 465-479.

Yellappa, T., Chetty, T.R.K., Tsunogae, T., Santosh, M., 2010. The Manamedu Complex: Geochemical constraints on Neoproterozoic suprasubduction zone ophiolite formation within the Gondwana suture in southern India. Journal of Geodynamics 50, 268-285.

FIGURE CAPTIONS

1. (a, b) Geology of the East African Orogen within Gondwana modified after Fitzsimons and Hulscher (2005). Line of cross-section X–Y indicated. The Bangweulu Block (BB) and Tanzania Craton (TC) are both part of the Congo Craton, separated by intracratonic deformation along the Ubendian Belt.. Also marked on the map are Betsimisaraka Suture (BMS), Tanzanian Arc/Vohibory Group (TZA), Palghat Cauvery Shear System (PCSS) and the Southern Granulite Terrane (SGT). Gondwana fit after Reeves *et al.* (2002). (c) Geology of Southern India indicating the area of this study. (d) Local map of the Madurai Block showing the sample localities (marked by white stars) and other UHT outcrops within the area. (e) Schematic east –west section through the East African Orogen showing the relationships between the main blocks.

2. Sequence of tectonic cartoons schematically illustrating the main interactions of crustal blocks during the amalgamation of Gondwana between 640 and 530 Ma. Block abbreviations: TC—Tanzania Craton; WGD—Western Granulite domain, Tanzania; MB—Madurai block; AN—Antananarivo block; NMB—northern Madurai block; SMB—southern Madurai block; TB— Trivandrum block. Figure modified from Plavsa et al. (2014).

3. P–T diagram illustrating the P–T paths as per previous studies of the Trivandrum and Madurai Blocks. Most studies are consistent with a clockwise evolution that passes through the UHT field. Abbreviations, study and locations as follows, B96 - Brown and Raith, (1996) - Perumalmalai; R97 - Raith *et al*., (1997) - Perumalmalai; S04 - Sajeev *et al*., (2004) - Ganguvarpatti; S06 – Sajeev *et al* (2006) - Kodaikanal; B07 - Braun *et al*.,

(2007) - Mottamala; K09 - Kondou et al., (2009) - Ganguvarpatti; T10 - Tsunogae and Santosh, (2010b)- Rajapalayam; S00 - Satish-Kumar, (2000) - Kannisseri; N07 - Nandakumar & Harley, (2000) - Kozhencherry; Braun *et al*., (1996) - Manali; T04 - Tatieshi *et al*., (2004) - Rajapalayam; T07 - Tadokoro *et al*., (2007) - 38km from Kodaikanal; Tm04 - Morimoto *et al.,* (2004) - Chittikara.

4. Field relationships and photomicrographs from Usilampatti. (a) Evidence for melt segregation at the outcrop scale with residuum material wrapped by leucosome rich layers. (b) Deformed leucosome and residuum with fabric wrapping porphyroblastic garnet (g) in a moderately deformed layer. (c) Corona of cordierite (cd) surrounding garnet in a moderately deformed leucosome-rich layer. (d) Sillimanite (sill)-rich domain showing porphyroblastic garnet wrapped by leucosome material. (e) Cordierite moats separating the coarse grained peak assemblage of garnet, ilmenite (ilm) and sillimanite. Note the pleochroic haloes within cordierite that contain small zircons (zrc). (f) Biotite (bi), sillimanite and quartz inclusions within a garnet porphyroblast.

5. (a-b) Photomicrographs of the textural position of zircon within the Usilampatti metapelite. (c-k) Cathodoluminesence images of the individual zircons that have undergone SHRIMP U-Pb analyses, individual spot analyses and ages are indicated and the results are tabulated in supplementary data Table 1.

6. Photomicrographs of the textural position of monazite from a sample of the Usilampatti metapelite. (a) Backscattered electron image of the area of thin section where monazite is intergrown with the peak minerals garnet, ilmenite and surrounded

by a corona of later cordierite and biotite. The white boxes are areas that have been electron probe mapped for Yttrium. (b-g) Yttrium elemental maps of monazite that have undergone SHRIMP U-Pb analyses, individual spot analyses and ages are indicated and the results are tabulated in supplementary data Table 2.

7. Field relationships and photomicrographs from Kodaikanal. (a) Migmatitic garnet-biotite gneiss with an abundance of late biotite, (b) foliated garnet-cordierite gneiss, (c) garnet with quartz inclusions, rimmed by cordierite and late biotite, (d) garnet with oriented sillimanite and biotite inclusions, magnetite contains exsolved spinel and cordierite forming at the expense of garnet.

8. Cathodoluminesence images of the individual zircons that have undergone SHRIMP U-Pb and LA-ICPMS REE analyses showing core and rim relationships. Results are tabulated in Supplementary Data Table 1.

9. Photomicrographs of the textural position of monazite from a sample of the Kodaikanal metapelite. (a) Backscattered electron image of the area of thin section where monazite is intergrown with ilmenite (ilm), (b) monazite inclusion within garnet. (b-c) Yttrium elemental maps of monazite that have undergone SHRIMP U-Pb analyses, the results are tabulated in Supplementary Data Table 2.

10. Pseudosection calculated in the NCKFMASHTO system for sample I06-62. Whole rock composition determined by XRF and converted to mol. % (reported on the top of the diagram, Fe^{2+}/Fe^{3+} determined by titration, H_2O equivalent to LOI). Red dashed lines are contours of the mol.% melt.

11. Pseudosection calculated in the NCKFMASHTO system for sample I06-79. (a) Whole rock composition determined by XRF and converted to mol. % (reported on the top of the diagram), Fe^{2+}/Fe^{3+} determined by titration. (b) *T-MH_2O* section to assess the effect of H_2O on the stability of the peak field. Red dashed lines are contours of the mol. % garnet.

12. Terra-Wasserburg concordia plots for all zircon analyses from (a) I06-62 and (b) I06-79.

13. Terra-Wasserburg concordia for geochronological analyses of all metamorphic monazite and zircon (a) I06-62 monazite, (b) I06-62 zircon, (c) I06-79 monazite, and (d) I06-79 zircon.

14. Normalised rare earth element plots for (a) I06-62 zircon, (b) I06-62 garnet, (c) I06-79 zircon, and (d) I06-79 garnet

15. Normalised rare earth element plots for (a) I06-62 monazite, and (b) I06-79 monazite.

16. (a) The configuration of the 1D model setup pre-thickening, immediately post thickening and 120 My after thickening. (b) 1D transient to steady state thermal models with varying heat production and P-T-t paths for particles with initial depths of 35 km, 50 km and 70 km. Grey boxes are the peak temperature fields as defined by the pseudosections in Figures 10 and 11. Model parameters and tabulated in Table 1.

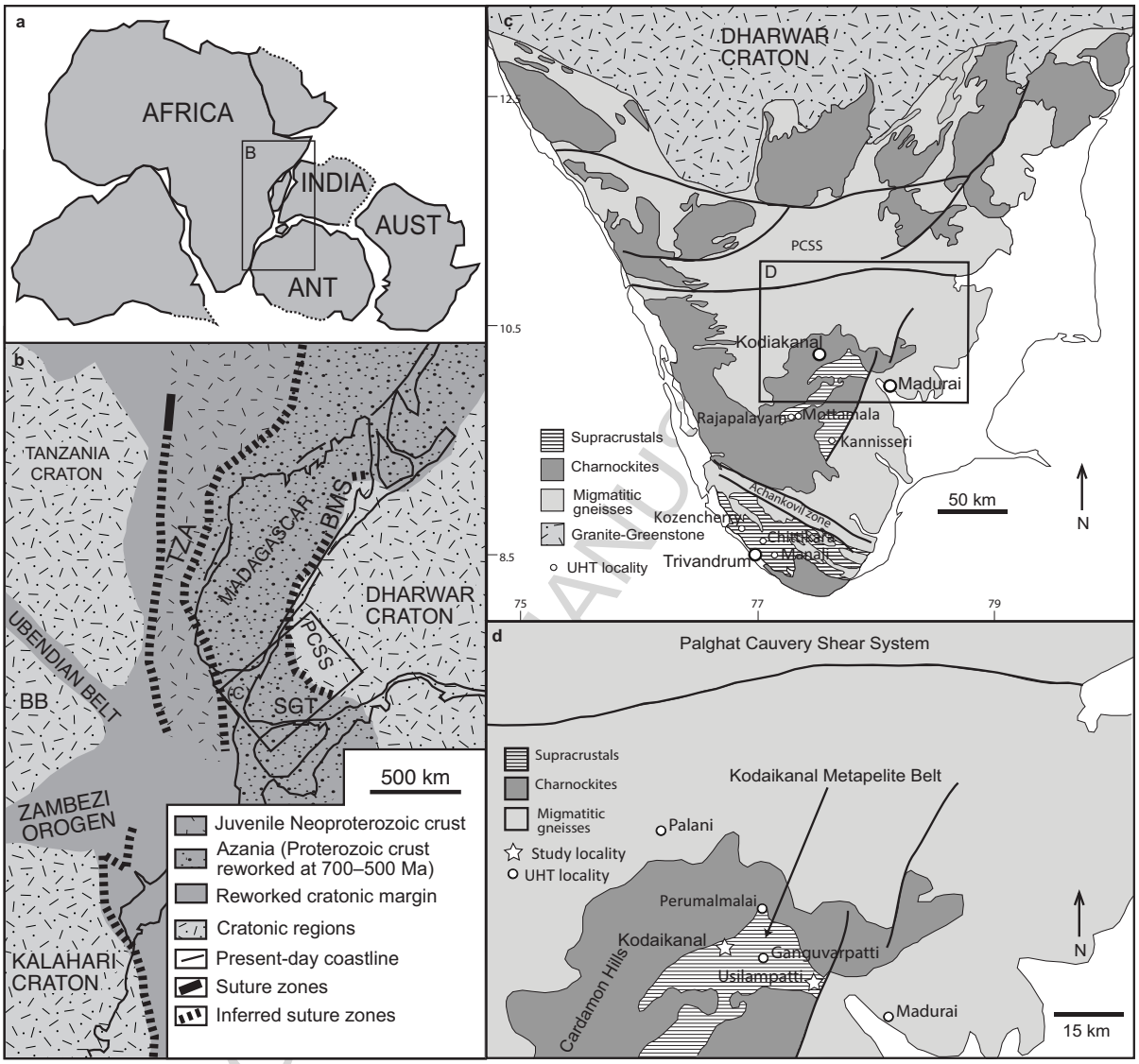

Figure 1

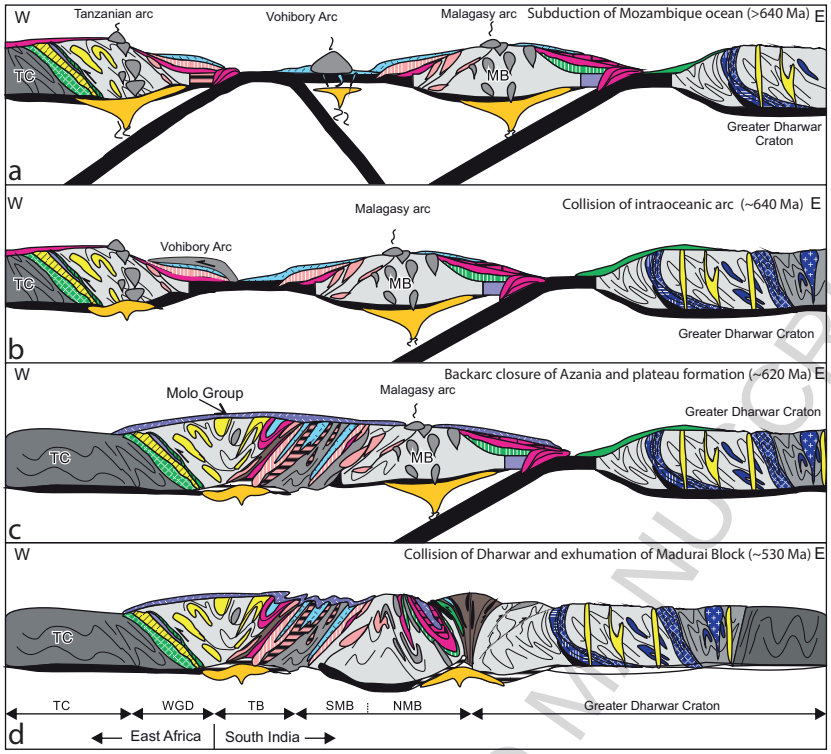

Figure 2

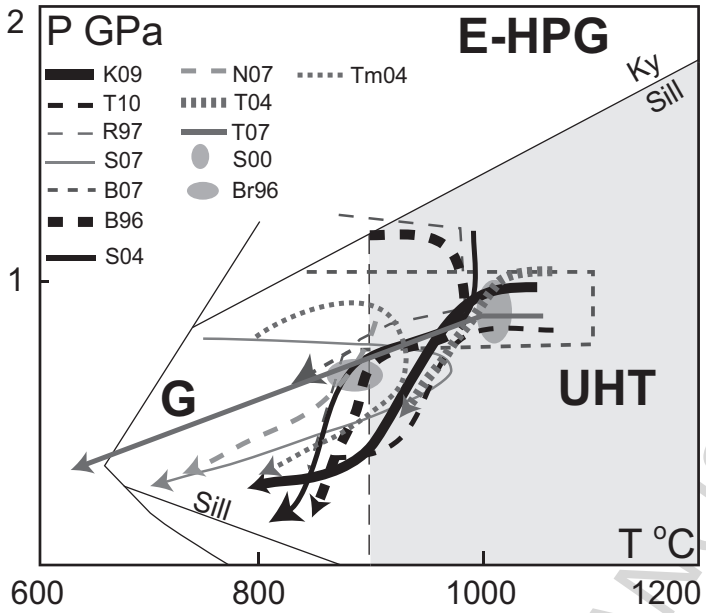

B96 - Brown & Raith, 1996 - Perumalmalai; R97 - Raith et al., 1997 - Perumalmalai; S04 - Sajeev et al 2004 - Ganguvarpatti; S07 - Sajeev et al 2007 - Kodaikanal; B07 - Braun et al., 2007 - Mottamala; K09- Kondou et al., 2009 - Ganguvarpatti; T10 - Tsunogae and Santosh, 2010b - Rajapalayam; S00 - Satish-Kumar, 2000 - Kannisseri; N07 - Nandakumar & Harley, 2000 - Kozhencherry; Braun et al., 1996 - Manali; T04 - Tatieshi et al., 2004 - Rajapalayam; T07 - Tadokoro et al., 2007 - 38km from Kodaikanal; Tm04 - Morimoto et al., 2004 - Chittikara.

Figure 3

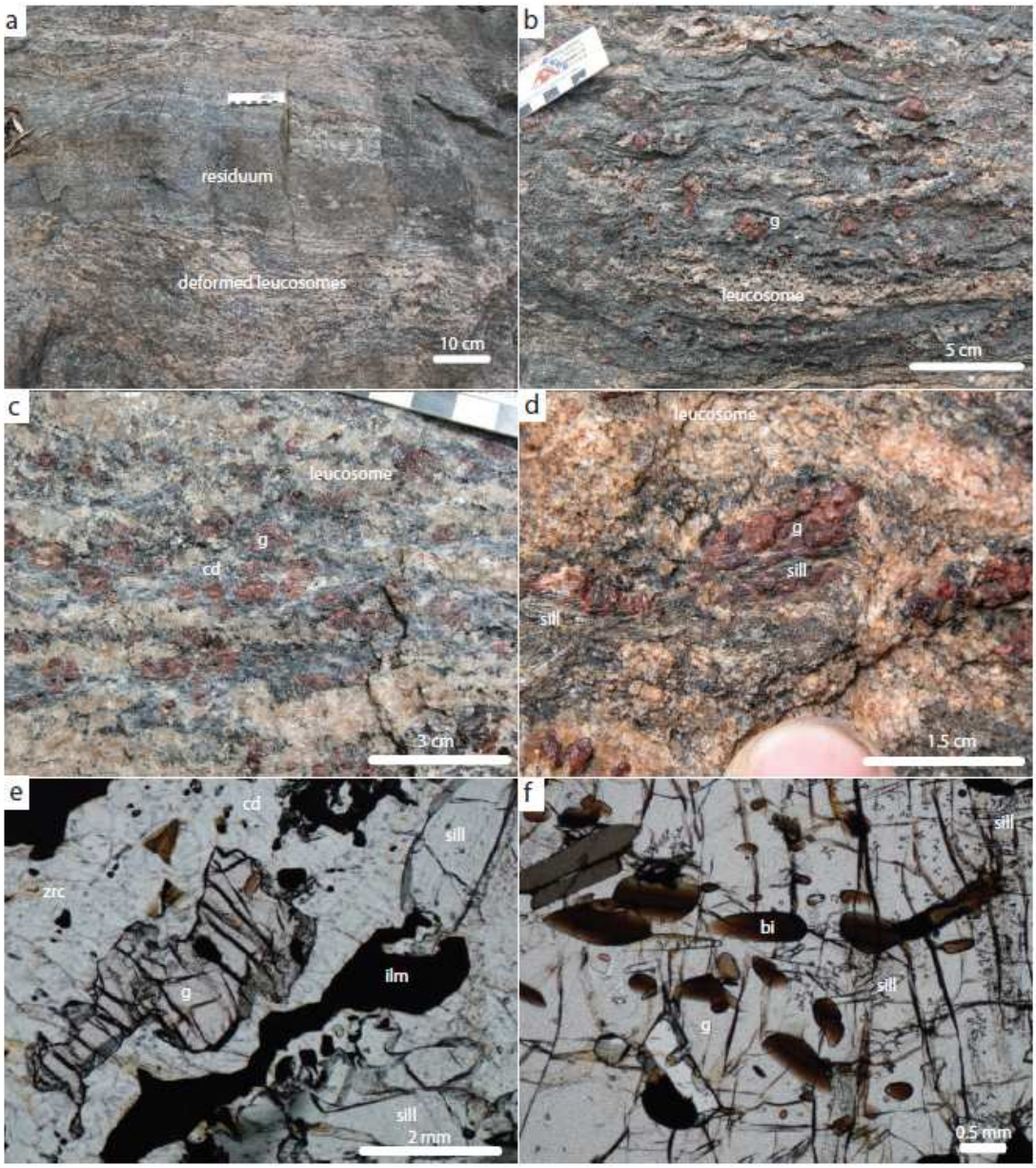

Figure 4

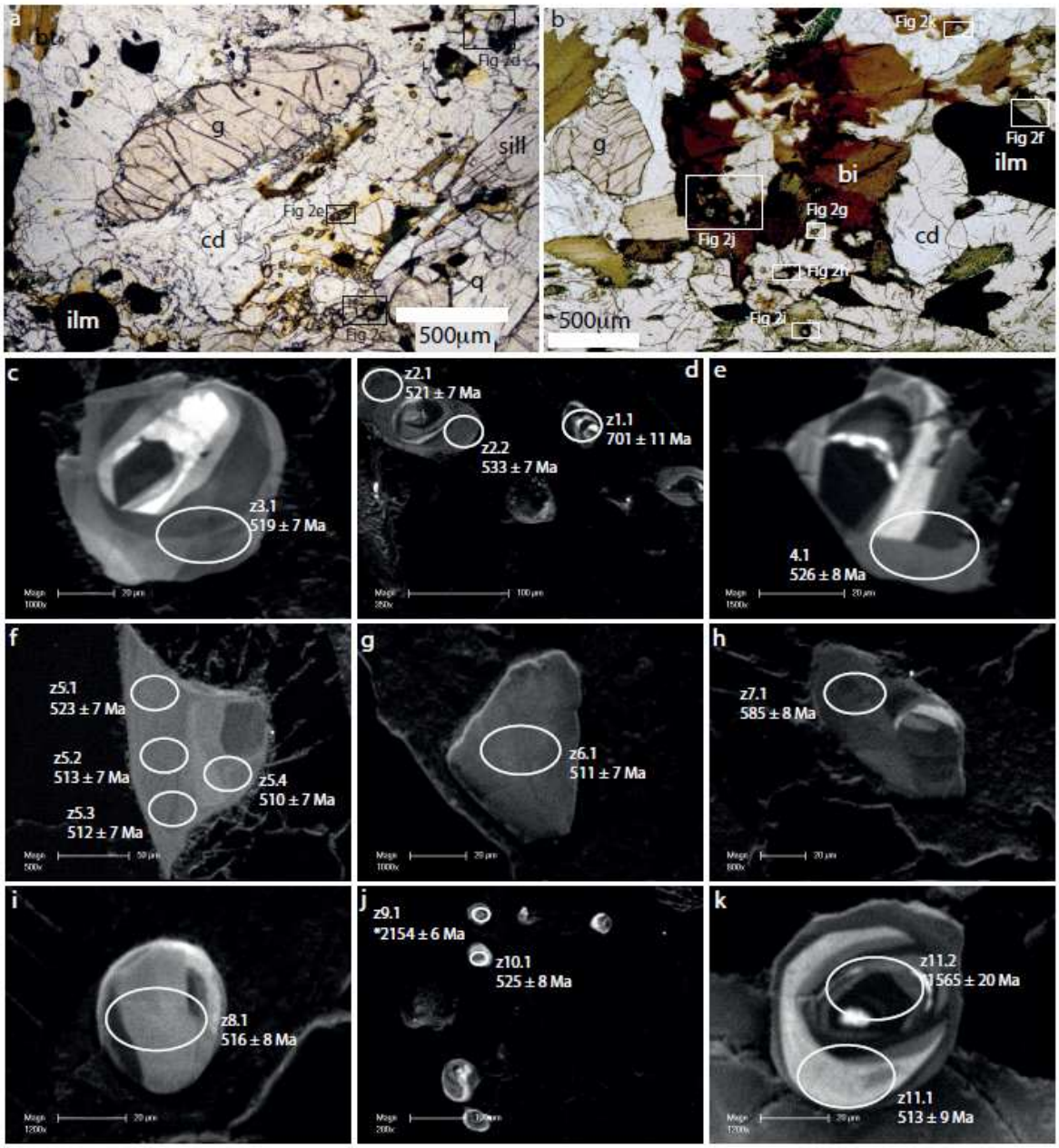

FIGURE 5

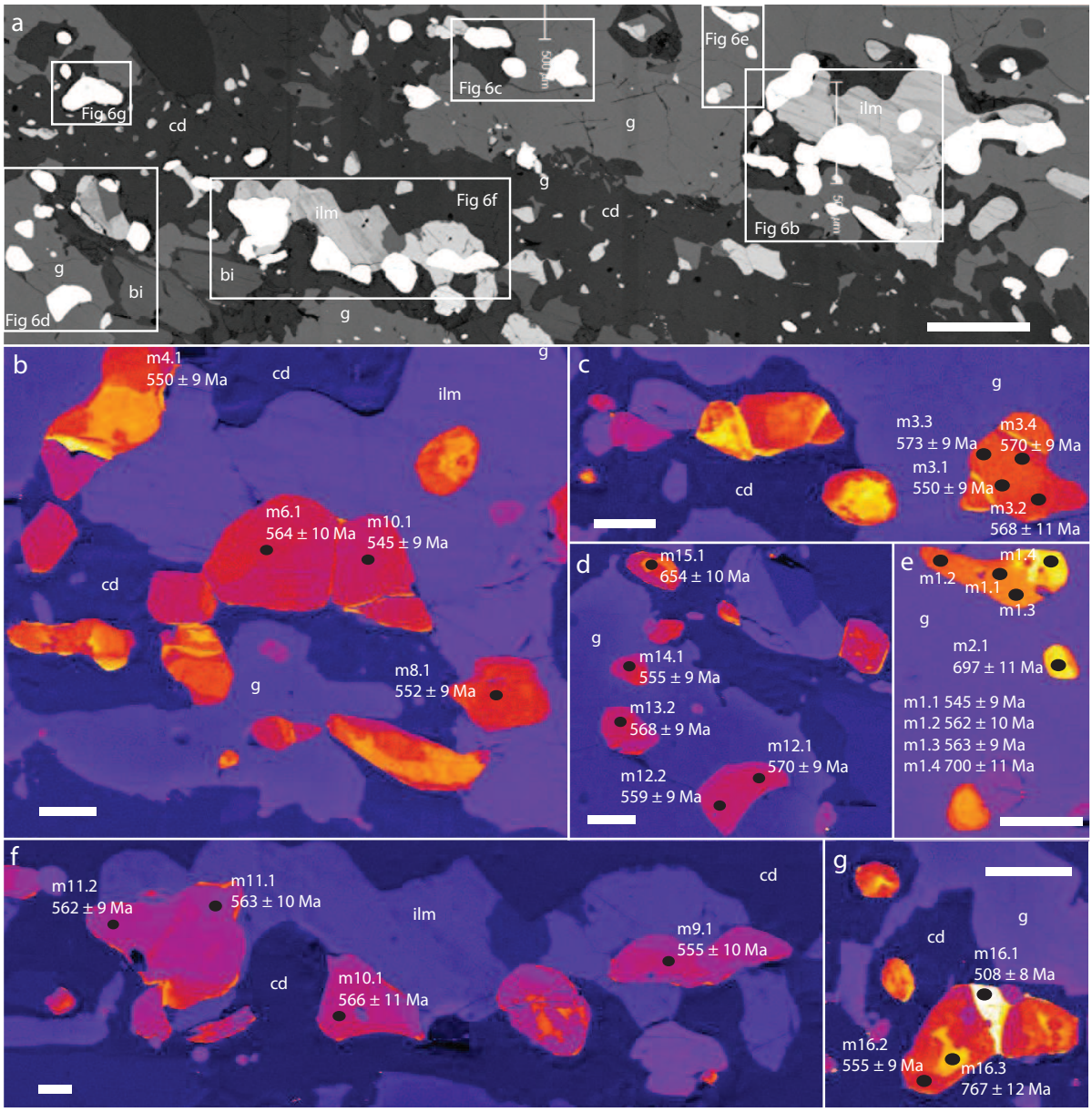

FIGURE 6

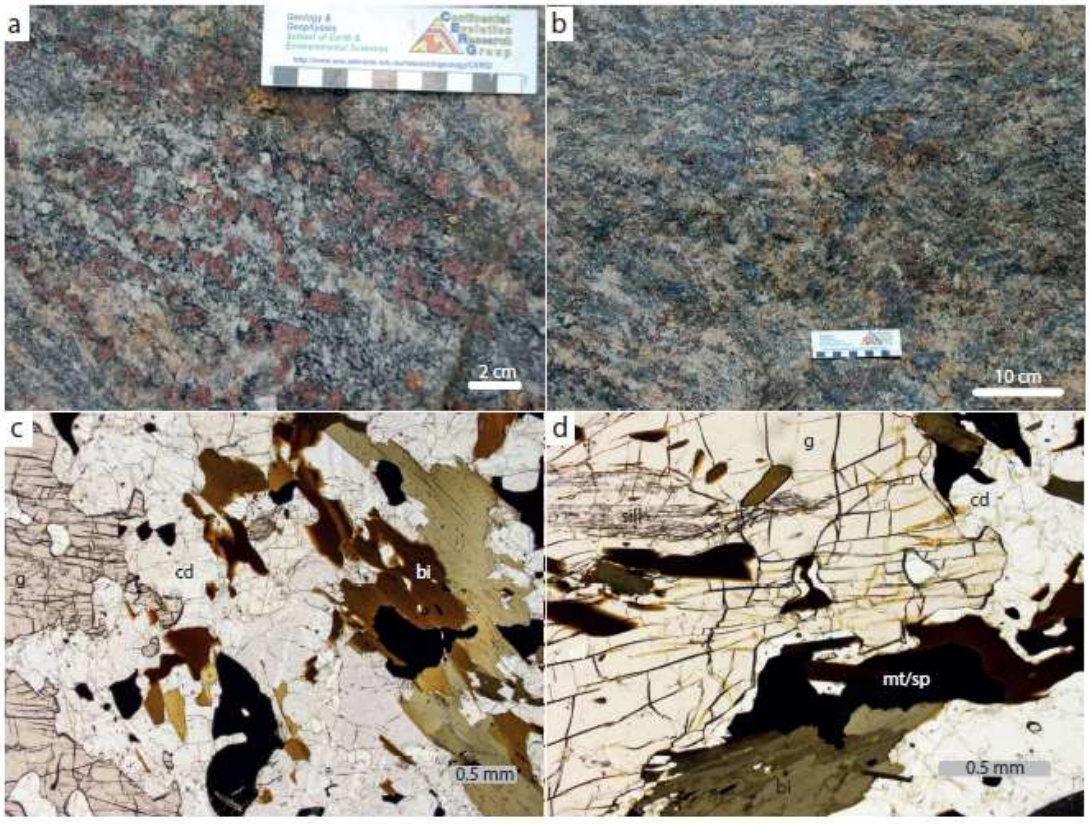

Figure 7

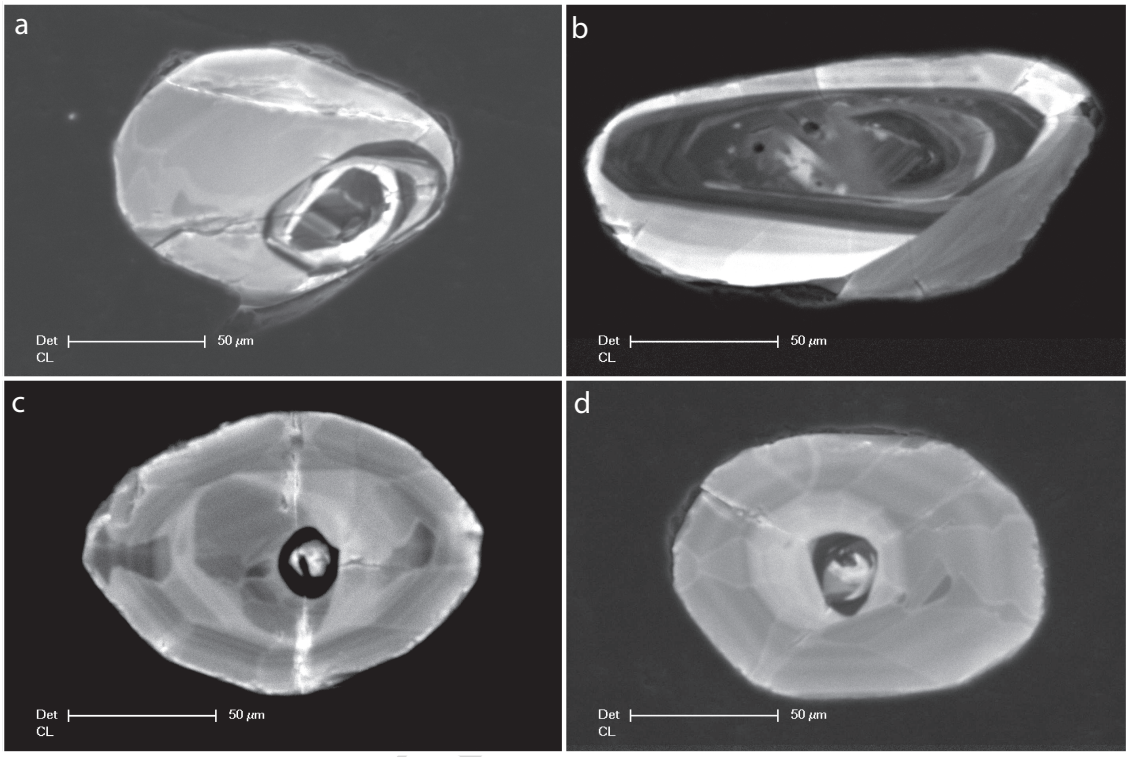

Figure 8

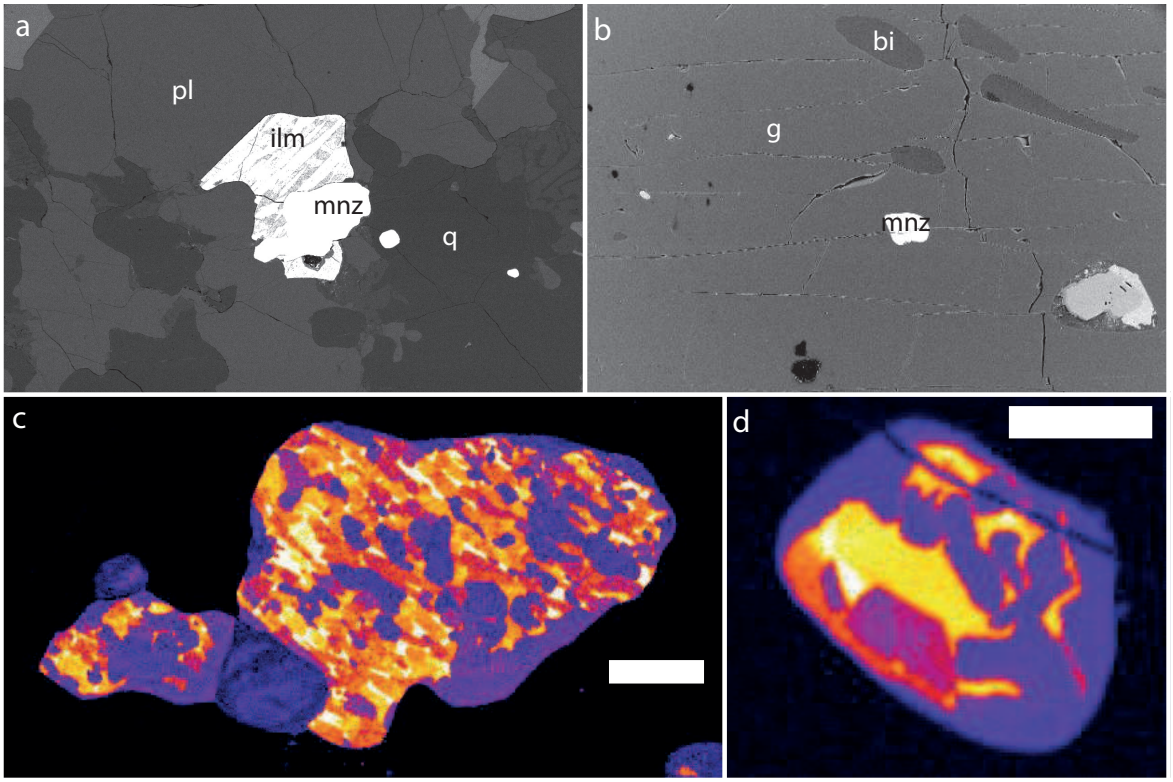

Figure 9

H2O	SiO2	Al2O3	CaO	MgO	FeO	K2O	Na2O	TiO2	O
0.69	64.17	13.37	0.72	6.74	11.60	0.95	0.26	0.57	0.94

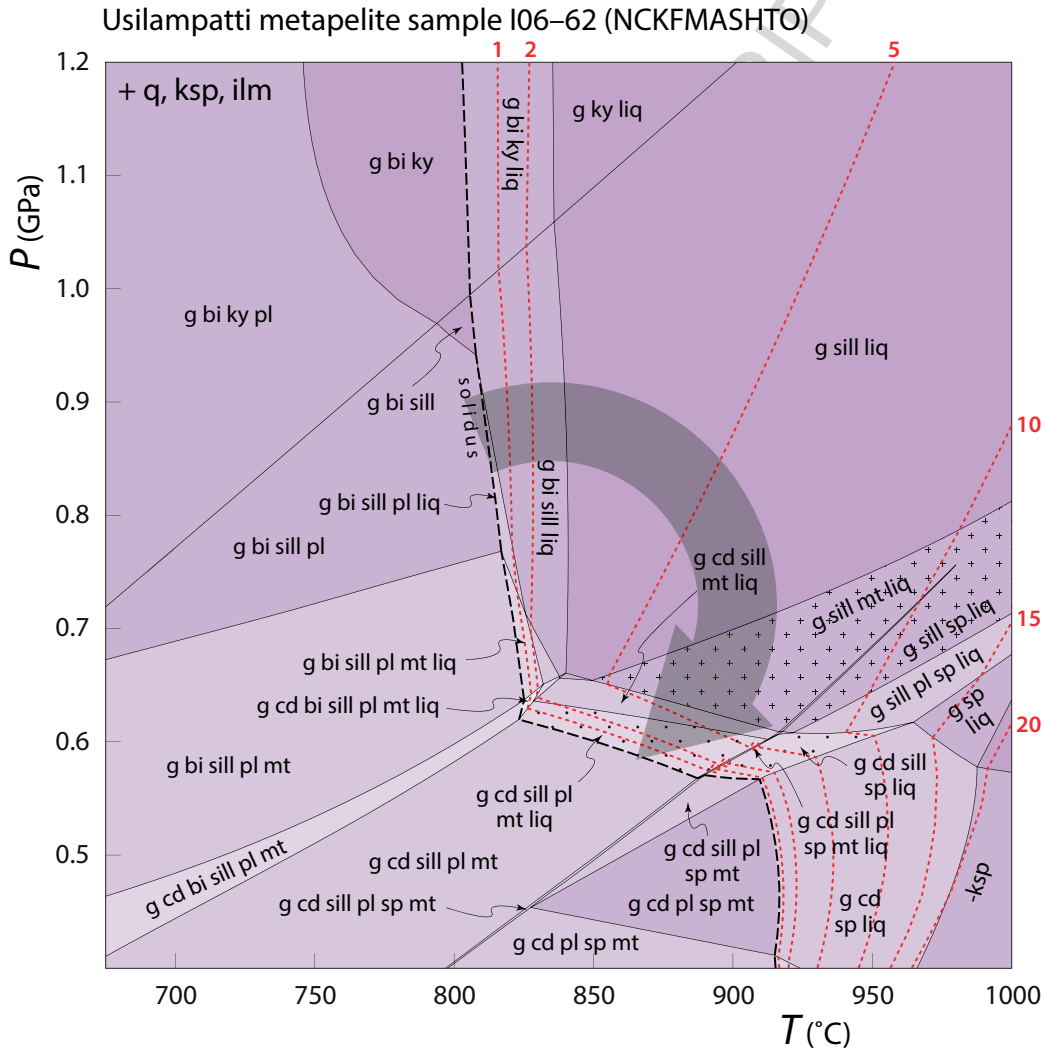

Figure 10

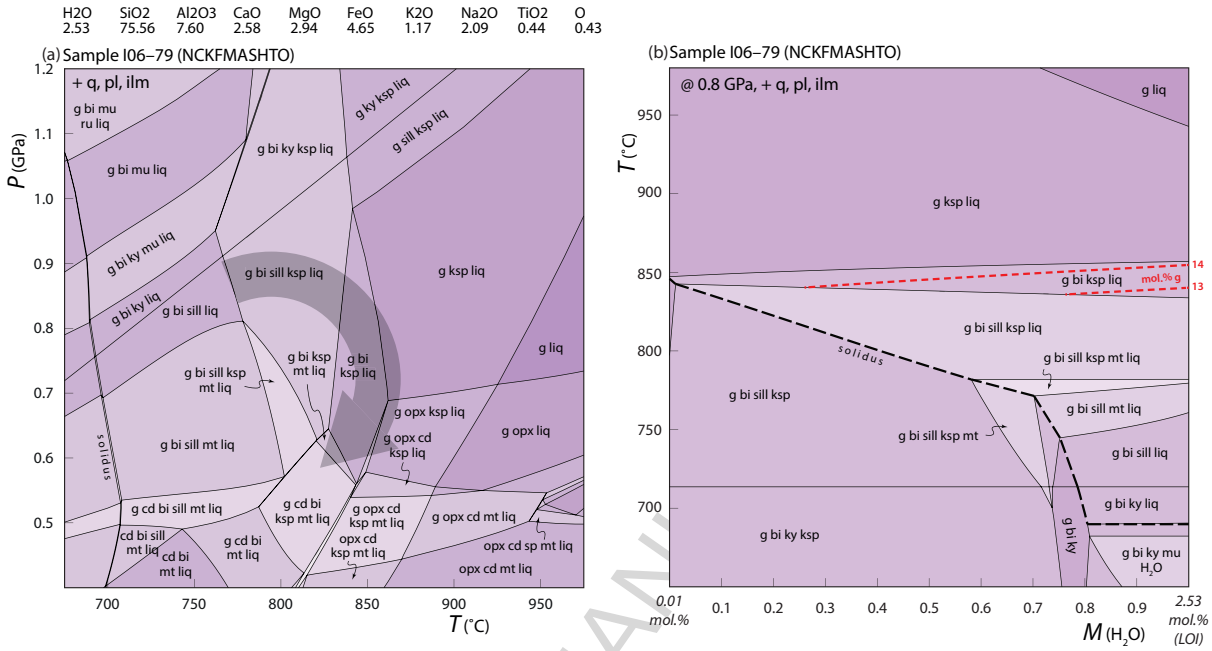

Figure 11

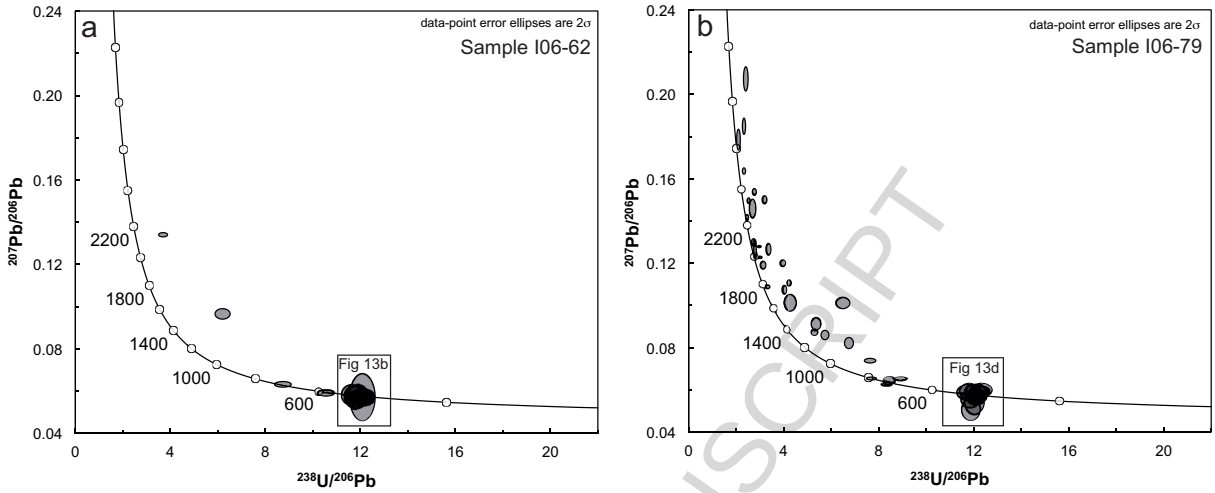

Figure 12

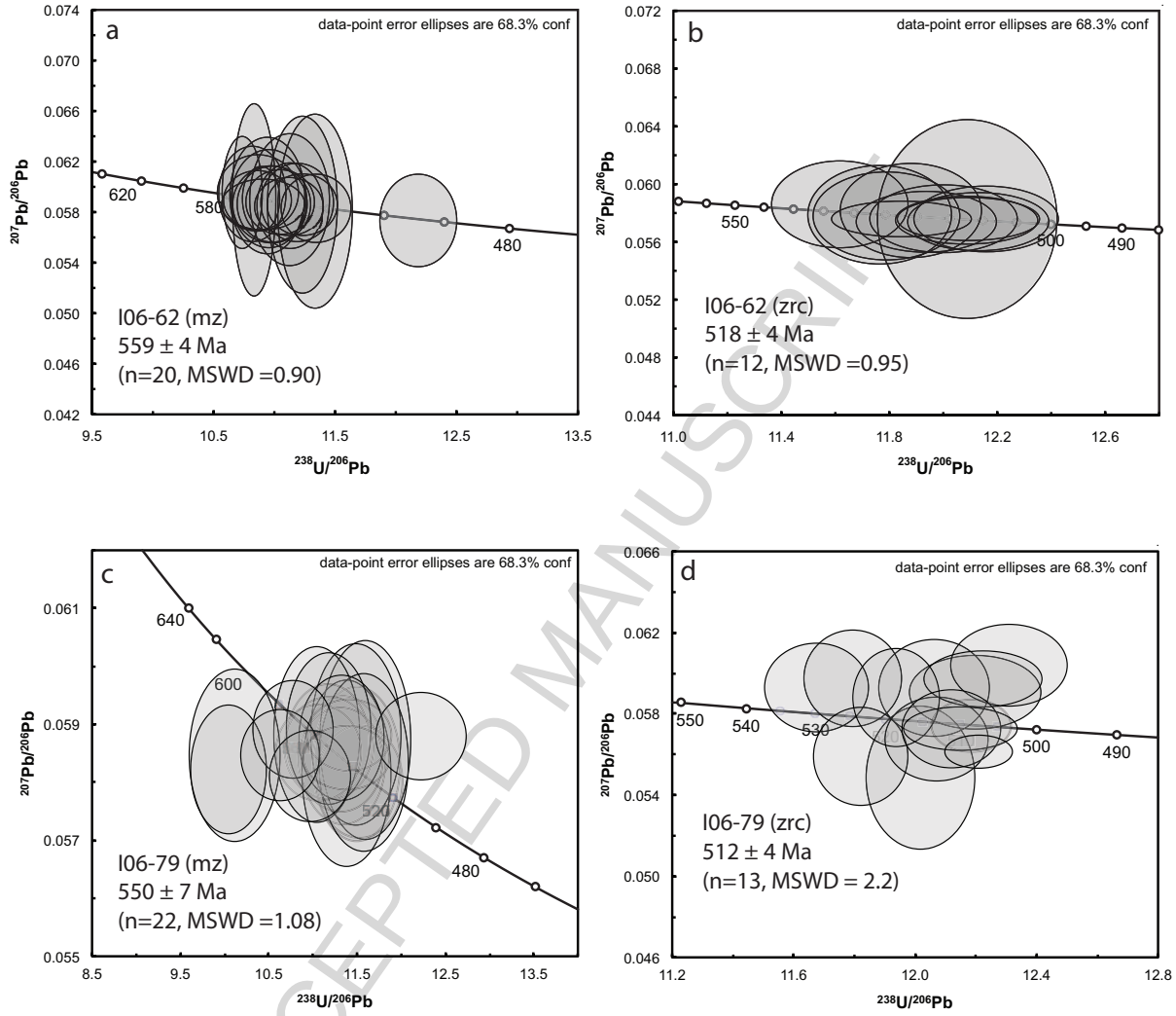

Figure 13

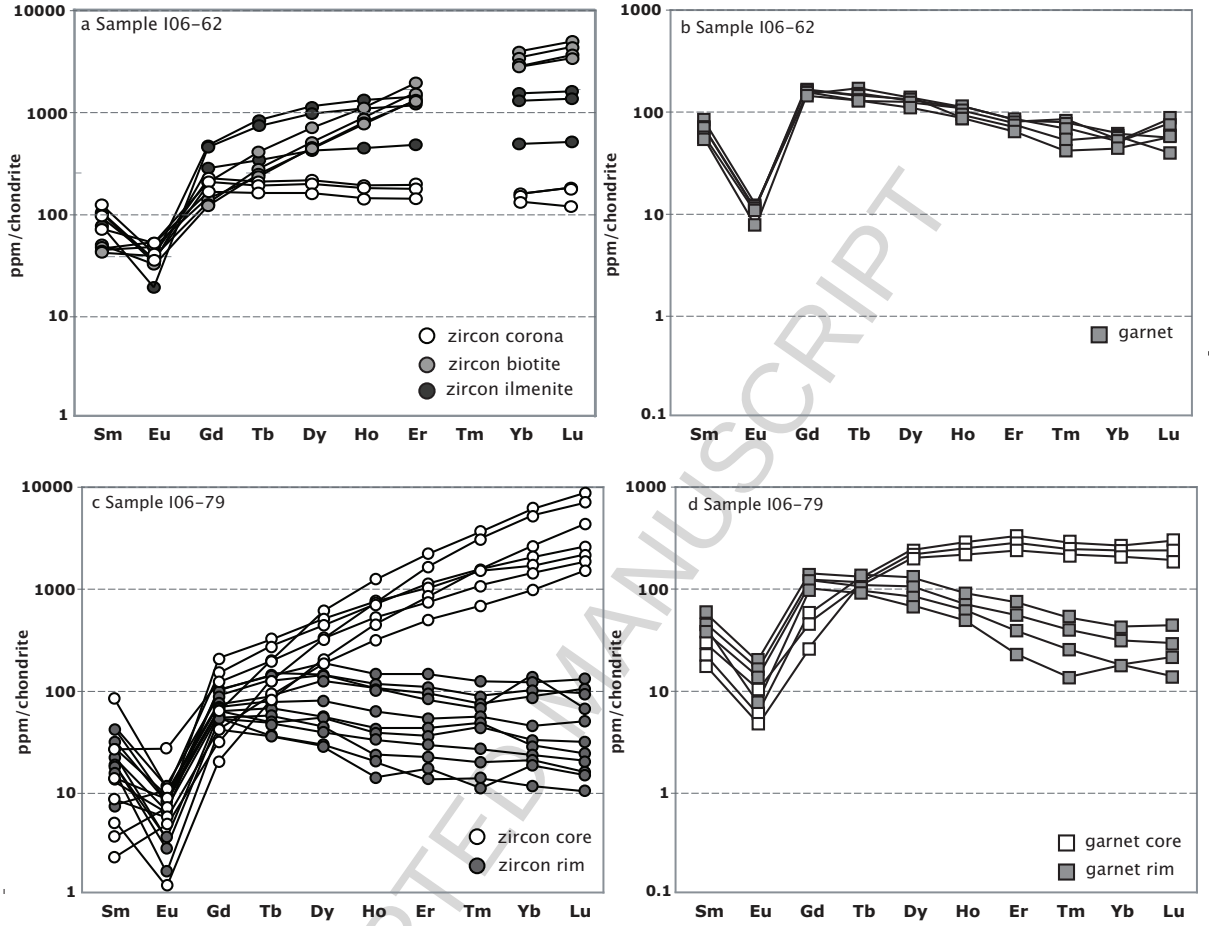

Figure 14

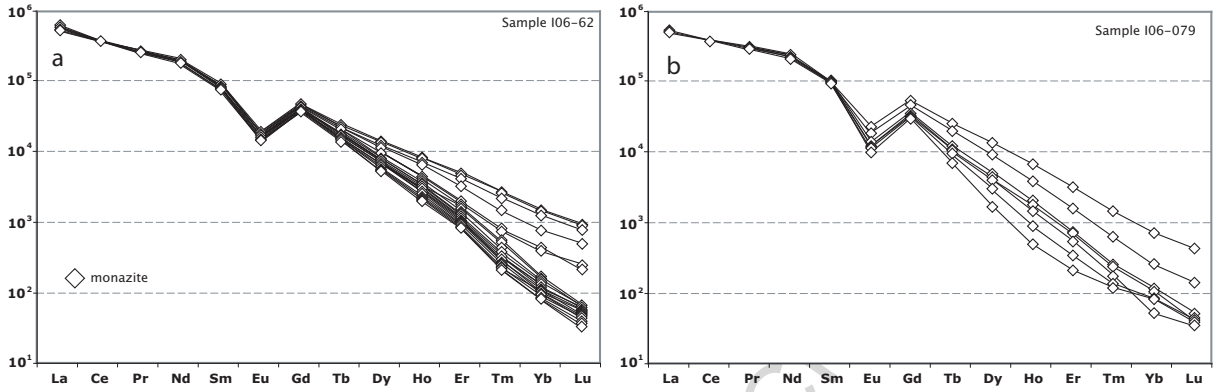

Figure 15

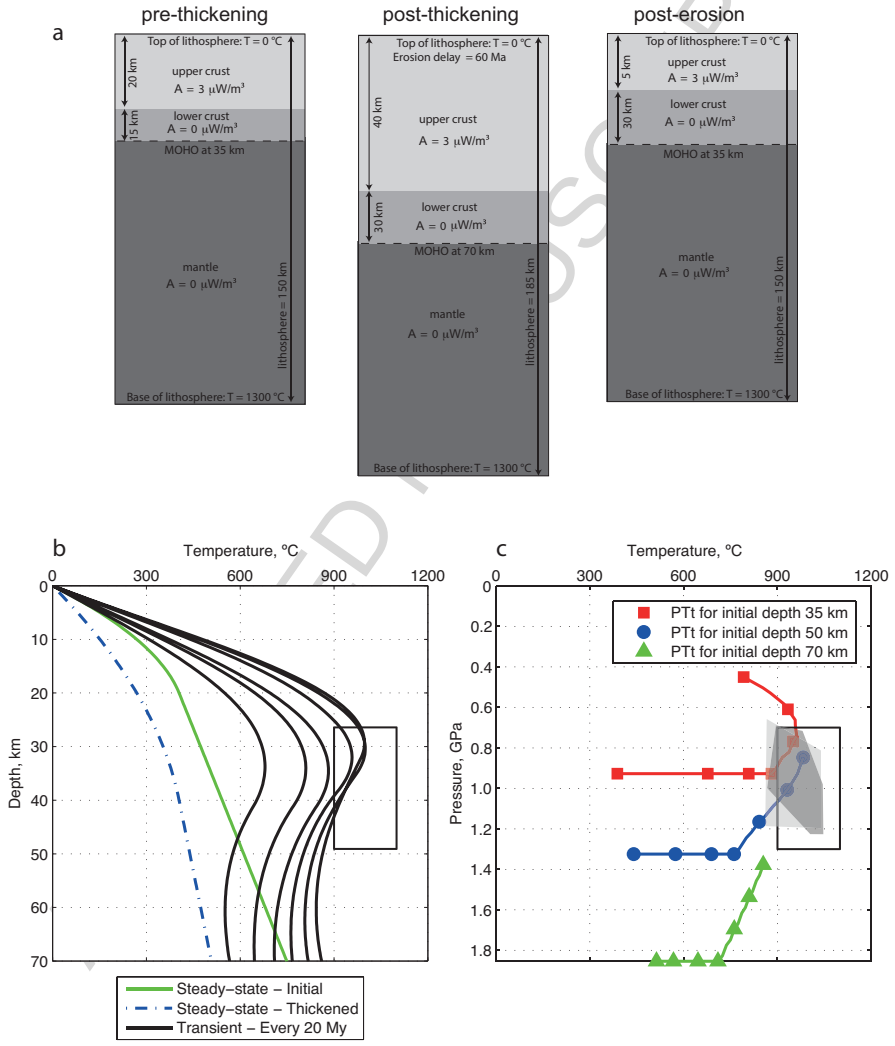

Figure 16

Table 1: Parameters used in 1D numerical model.

A_{rad} 0-25 km (μWm^{-3}) - crustal heat production	3
L (kJ Kg^{-1}) – latent heat of partial melting	320
α (from Stüwe, 1995)	0.0001
T_{min} - T_{max} (°C) – interval over which rocks generate partial melt	650 - 1100
U (mm/yr) - erosion rate (after delay of 60 Ma)	0.6
Initial conductivity @ 25 °C (W m^{-1} K^{-1})	2.5

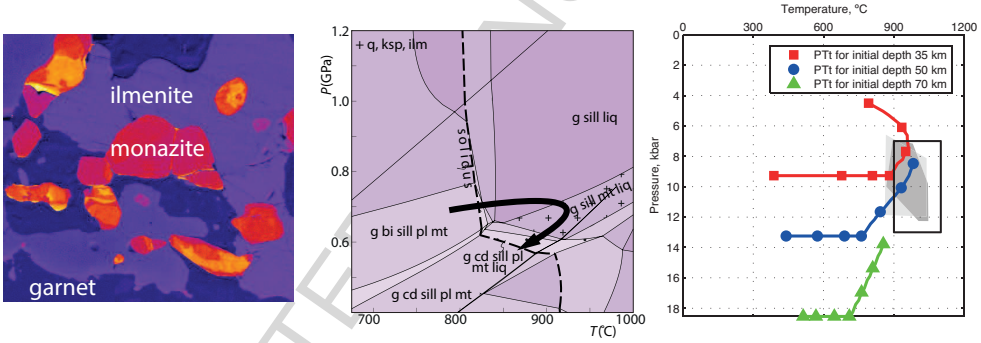

Graphical Abstract

Research Highlights

- High-temperature metamorphism in the Madurai Block lasted ~ 100 My
- Radiogenic heating was the main source of heat
- Regional-scale UHT metamorphism can be linked to the supercontinent cycle